Different Water Networks Confined in Unidirectional Hydrophilic Nanopores and Transitions with Temperature

Frederico Alabarse, Benoît Baptiste, Mónica Jiménez-Ruiz, Benoit Coasne, Julien Haines, Jean-Blaise Brubach, Pascale Roy, Henry Fischer, Stefan Klotz, Livia Bove

Different Water Networks Confined in Unidirectional Hydrophilic Nanopores and Transitions with Temperature

Frederico G. Alabarse[†§], Benoît Baptiste[†], Mónica Jiménez Ruiz[♦], Benoit Coasne[♣], Julien Haines[‖], Jean-Blaise Brubach[▽], Pascale Roy[▽], Henry E. Fischer[♦], Stefan Klotz[†], Livia E. Bove[†#]**

† Institut de Minéralogie, de Physique des Matériaux et de Cosmochimie, Sorbonne Université, Paris, France.

§ Elettra Sincrotrone Trieste, Basovizza, Trieste, Italy.

♦ Institut Laue-Langevin, Grenoble, France.

♣ Univ. Grenoble Alpes, CNRS, LIPhy, 38000 Grenoble, France.

‖ ICGM, CNRS, ENSCM, Université de Montpellier, Montpellier, France.

▽ Synchrotron Soleil, Saint Aubin – BP48, Gif sur Yvette, France.

Dipartimento di Fisica, Università di Roma la Sapienza, Roma, Italy.

ABSTRACT

The structure and vibrational properties of water molecules confined in unidirectional hydrophilic nanopores of $AlPO_4$-54•xH_2O were investigated from room temperature down to 10 K by single crystal synchrotron X-ray diffraction, neutron pair distribution function analysis, incoherent inelastic neutron scattering, far- and mid-infrared spectroscopy, ab-initio Molecular Dynamics and Grand Canonical Monte Carlo Simulations. The ensemble of results indicates that water confined in $AlPO_4$-54•xH_2O nanopores does not crystallize down to 10 K and points at the existence of two different types of water networks, whose local arrangement and dynamical behavior become more and more distinguished when lowering the temperature below 150 K. The dependence of temperature of the infrared spectroscopy points at two transitions at 250 and 150 K. Upon cooling, water close to the zeolite pore wall shows a highly ordered local arrangement induced by the pore wall, with more defined site occupancy and lower density with respect to bulk water. Conversely, water in the pore core shows a denser, more disordered and orientationally distorted arrangement, and a glassy-like behavior down to the lowest investigated temperature.

TOC Figure:

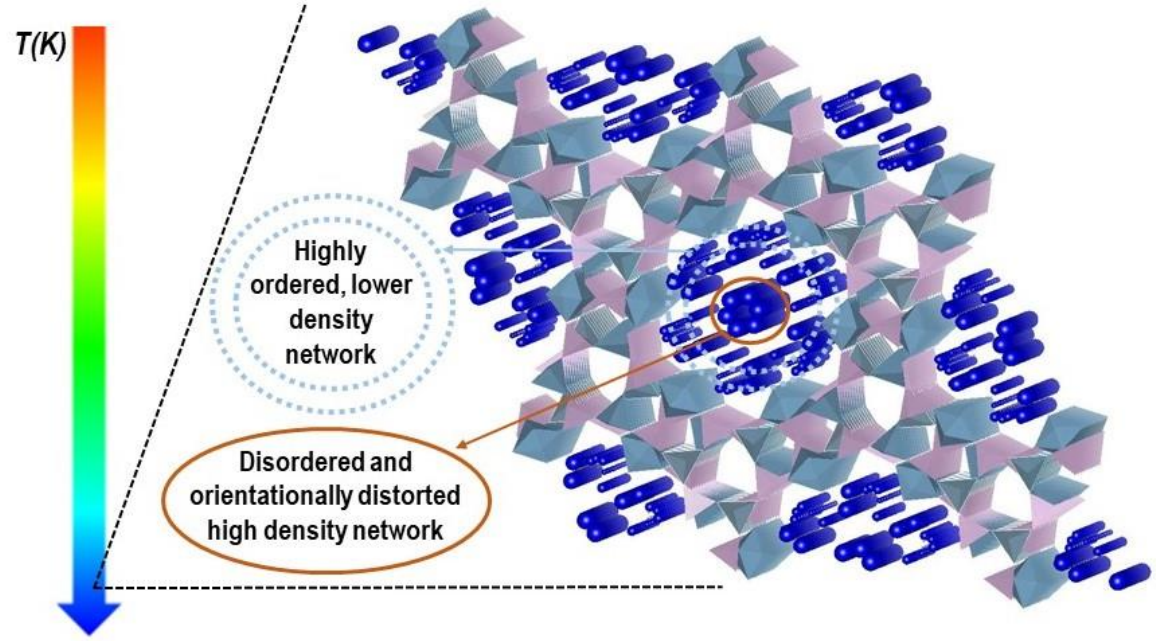

1. Introduction

The ordering of small molecules inserted in nanoporous channel systems is of great interest for applications such as molecular sieves, phase separation and heterogeneous catalysts [1], nanotribology [2], fabrication of nanomaterials using H_2O as a template [3] or even for the durability of concrete [4]. As water is normally present in most molecular sieves, its order and reactivity as a function of temperature is clearly of particular importance in chemistry, geology, biology, and physics. Whatever the nature of the surface of the porous matrix (hydrophilic or hydrophobic), the restriction of the accessible space induced by nano-confinement has important structural, dynamical and thermodynamic consequences [5]. Over the past two decades a series of studies have been done on water confined in different nanoscopic porous materials [6-11], both crystalline and amorphous, and have indicated the universal lowering of water freezing point, while no general agreement has been reached on the conditions of suppression of crystallisation by confinement, in terms of pore size, pore structure, and nature of the water-surface interaction. As an example, the use of Mo-based nanocapsules, which contain a large number of pores, was used as nanocontainers /nanosponges to study water confined in strong confinement [12]. The authors have shown that, by changing the chemical composition of the internal cluster shell, it was possible to influence the structures of encapsulated nanodrops of water. Another example concerns the very recently reported ordering of water wetting-layer in single-walled aluminogermanate imogolite nanotubes [13]. Some studies have shown that, for temperatures below the bulk freezing point, water confined in hydrophobic nanopores crystallizes [6-9]. Such phenomenon is also supported by studies which show the formation of ice nanotubes in carbon nanotubes [8,9]. A different scenario was reported concerning the freezing of water in hydrophilic nanopores: the pore surface can induce orientational order of water in contact with its wall (*proximal water*), while water in the pore center (*inner water*) is more disordered [14]. Crystallization of proximal water is suppressed as the number of hydrogen bonds (HB) formed is insufficient, while crystallization of the inner water is believed to be hindered as the curvature prevents the formation of a network of tetrahedrally coordinated molecules.

Water confined in the nanopores of hydrophilic $AlPO_4$-54•xH_2O has been the subject of several recent studies involving variable pressure-temperature conditions [14-18]. $AlPO_4$-54•xH_2O (hexagonal VFI structure, space group $P6_3$, a = 18.9678(13) Å and c = 8.0997(4) Å, $Al_{18}P_{18}O_{72}$•xH_2O) [17] exhibits highly hydrophilic 1-D pores along the **c** direction, with a diameter of 12.7 Å that are among the *largest pores known for zeolites and aluminophosphates*. In the pores, H_2O molecules form a disordered hydrogen-bonded network at ambient temperature and pressure. $AlPO_4$-54•xH_2O thus represents an interesting target material to study nanoconfined water under strong confinement. The zeolite framework is built up of 4, 6 and 18-membered rings of alternating AlO_6, AlO_4 and PO_4 polyhedra. One-third of the aluminium cations are octahedrally coordinated due to the presence of two H_2O molecules in their coordination sphere. Previous synchrotron single crystal structural studies at ambient pressure and temperature reported the presence of 36 water molecules in its pores, with 11 further H_2O molecules identified by Molecular Dynamics simulations that were considered too mobile to be detected by X-ray diffraction [17]. The dehydration of $AlPO_4$-54•xH_2O was recently studied *in situ* as a function of vacuum pressure at room *T* [19]. While previous studies indicate that $AlPO_4$-54•xH_2O contains close to 24 wt% H_2O [20] corresponding to an *x* value of about 2.14, it has been shown that when the material is exposed to primary vacuum (5 Pa) pore water is rapidly removed and *x* drops to 0.25 and *x*= 0.12 when exposed to secondary vacuum (0.05 Pa) [19], both values refering to some amount of structural water remaining in the Al polyhedra. As a comparison, if only structural water remains in $AlPO_4$-54•xH_2O, then *x* would be 0.67. When pressure is applied using water itself as pressure transmitting medium (PTM), super-hydration effects and hindering of pore collapse are observed, with a consequent major change in the mechanical properties of the system [15]. From a dynamical point of view, super-diffusion effects have been predicted to occur for water nanoconfined in the unidimensional pores [16]. Upon lowering the temperature at ambient pressure, full ordering of nanoconfined water was not observed down to 173 K [14] but water ordering and site occupancies of proximal water were shown to increase as the temperature decreases, likely because water molecules interact with the nanopore wall forming HB with O atoms of the framework.

Here we report a series of new experiments probing both structural and vibrational properties of H_2O in the above-mentioned hydrophilic nanopores down to 10 K by single crystal synchrotron X-ray and powder neutron diffraction measurements, incoherent inelastic neutron scattering, far- and mid-infrared spectroscopy, ab-initio Molecular Dynamics and Grand Canonical Monte Carlo Simulations. These new results clearly indicate that water in the zeolite nanopores does not crystallize even at the lowest investigated temperature and reveal an increasingly different structural and dynamical behavior from proximal to inner water on cooling: while proximal water shows an increase in the orientational order, as well as an increasing localization at the pore sites and a strengthening of the water-water interactions, inner water exhibits increasing disorder and an amorphous glass-like behaviour.

2. Materials and Methods

The ordering of water confined in the $AlPO_4$-54•xH_2O nanopores was investigated using two samples: small poly-crystals and large single crystals. The small poly-crystals (linear dimensions on the order of 30x1x1 μm^3) were synthesized from nanometric alumina (Pural SB) and phosphoric acid by an optimized sol-gel procedure followed by hydrothermal treatment as described previously [14,15]. The high quality single crystals (needle-like 200x25x25 μm^3) were synthesized from an alternative method using polyphosphoric acid, details can be found elsewhere [14]. The dehydrated phase ($AlPO_4$-54) was obtained by keeping the sample at 293 K and 10^{-6} mbar overnight. This room temperature treatment removes the pore water, while retaining a small amount of the water coordinated at the 6-fold Al [15,19].

X-ray diffraction (XRD) measurements on a $AlPO_4$-54•xH_2O single crystal were performed at 50, 100 and 135 K. The 50 K measurement (λ = 0.6717 Å) was carried out on the 4-circle diffractometer on the CRISTAL beamline (SOLEIL Synchrotron / Gif-sur-Yvette) using a Cryo Industries of America He gas stream cooler. A thin needle shaped crystal was selected in oil and mounted within a cryoloop. The intensities were collected from a phi scan with a 2D CCD detector placed at 80 mm from the sample using a 200x200 μm^2 beam size. The measurement at 100 K was realised at the XRD platform of the *Institut Parisien de Chimie Moleculaire* (IPCM, *Sorbonne Université*) on a 4-circle Bruker AXS Kappa-APEX II diffractometer (MoKα, λ = 0.71073 Å) using an Oxford Cryosystem N_2 Cryostream. The data at 135 K were collected at the Institute Charles Gerhardt Montpellier on a Bruker D8 Venture 4-circle diffractometer equipped with an Incoatec MoKα microsource and a Photon II detector and combined with an Oxford Cryosystem N_2 Cryostream. In all cases, data reduction, cell refinement, space group determination, scaling, and empirical or analytical absorption correction [21] were performed using CrysAlisPro software [22] or Bruker APEX3 software. The structures were solved in the hexagonal $P6_3$ space group through the Olex2 [23] program by direct methods using SHELXS [24]. The refinement was then carried out with SHELXL [25] by full-matrix least-squares minimization and difference Fourier methods. All non-Hydrogen atoms were refined with anisotropic displacement parameters. A merohedral twinning was detected and the refinement was then significantly improved considering the (0 1 0, 1 0 0, 0 0 − 1) twinning matrix. The R_1 factor (see Table S1 at the SI-Section 2) decreased from

13.90% to 3.39% and from 14.2% to 4.11% for the data collected at 100 and 50 K, respectively. A R_1 factor of 3.31% was obtained for the data at 135 K.

Neutron scattering data for pair distribution function (PDF) analysis were collected in the range of *T* = 10-300 K from 332 mg of $AlPO_4$-54•*x*H_2O powder loaded into a cylindrical vanadium can (5x20 mm sample diameter and height, respectively) on the D4 instrument (Institut Laue-Langevin/ Grenoble). PDF(*r*) gives the probability of finding an atom at a distance *r* from an average atom taken as the origin, its detailed definition and calculations formalities are described elsewhere [26,27]. D4 is a two-axis diffractometer, equipped with nine 1-D position-sensitive microstrip detectors pressurized with ^{3}He gas to 15 bar for efficient detection. The diffraction patterns were measured over a large *Q*-range (Q_{range} = 0.5-23.5 Å^{-1}) using a Cu220 monochromator selecting 0.5 Å wavelength incoming neutrons, and 2x2-horizontal slits, vertical diaphragm at 30 cm upstream from the sample, plus additional vertical slits at 5 cm upstream of sample as collimations. More information concerning D4 instrument can be found elsewhere [28]. Experiments were carried out on dehydrated and hydrogenated samples at 4 temperatures points (*T* = 10, 100, 173 and 300 K) at ambient pressure. The scattering data were collected over 1.5 h for *T* = 100, 173 and 300 K, and over 13.5 h for *T* = 10 K.

Inelastic neutron scattering (INS) measurements of the generalised density of states (*G*DOS) of water confined at $AlPO_4$-54•*x*H_2O were performed using the IN1-LAGRANGE spectrometer (ILL/ Grenoble) in a fixed-monitor regime with the 2D-focusing Cu220 monochromator. INS is an excellent technique to study water hydrogen bonding in confined media and it was already used in previous studies to provide information on librational modes in hydrated minerals [29-31]. The vibrational spectrometer LAGRANGE provides the high energy transfer needed to study the inter- and intra-molecular vibrations of water. The scattering intensity from both the hydrated and dehydrated sample was collected at *T* = 10, 173, 235 and 293 K, using a Displex closed cycle refrigerator. 242 mg of $AlPO_4$-54•*x*H_2O powder were loaded into an aluminium sachet to give the sample thickness of ~2 mm for the low temperature measurements. The data were collected over the range of 26-500 meV (172-4000 cm^{-1}). The most interesting results are those below 200 meV (1600 cm^{-1}), in the region of the water librational band. The

spectra were accumulated over 6 h for each temperature. More information concerning the IN1-LAGRANGE instrument can be found elsewhere [32,33].

Mid and far-Infrared (IR) spectra of $AlPO_4$-54•xH_2O at low temperatures in the T = 17-300 K range were collected at the Advanced Infrared Line Exploited for Spectroscopy beamline (AILES, Synchrotron SOLEIL/ Gif-sur-Yvette), which is equipped with a Bruker instruments IFS 125 FT-IR spectrometer modified to operate with the synchrotron source [34]. Mid-IR spectra (600–4000 cm^{-1}) were obtained with a MCT/InSb (600–5000 cm^{-1}) detector and a KBr beamsplitter. The far-IR domain was investigated using a 6 μm Mylar beamsplitter and a 4.2 K Si-bolometer detector (10–700 cm^{-1}). The spectra were acquired with a resolution of 2 cm^{-1} with 300 scans in both, far- and mid-IR. The AILES beamline is equipped with a Helium closed circuit cryostat (pulse tube refrigerator cold head model CryoMec PT405) placed in vacuum chamber set up pumped down to ~10^{-6} mbar. The cryostat allows reaching low temperatures in the T = 4-360 K range, the sample temperature was measured with an accuracy of about $\pm$ 0.1 K [35]. Measurements were acquired from low to high T. All mid- and far-IR measurements were performed in transmission mode, the sample being placed in a sealed cell with windows of CaF_2 and PE, respectively for the mid- and far-IR ranges. To avoid band saturation into the spectra, the sample powder was dispersed at 1% concentration in CdTe and at 10% concentration in polyethylene (PE), respectively for the mid- and far-IR measurements.

Grand Canonical Monte Carlo (GCMC) simulations were carried out to probe water adsorption at T = 10, 110, 173, 235 and 293 K in $AlPO_4$-54•xH_2O. Such technique is a statistical mechanics method that simulates a system with constant volume V (the pore with the adsorbed phase) in equilibrium with a fictive reservoir of water molecules imposing its chemical potential μ and temperature T. The pressure is obtained from the chemical potential μ according to the bulk equation of state for an ideal gas (which corresponds to a very good approximation for water at the temperatures considered here). Periodic boundary conditions are used along the 3 directions x, y, z to avoid finite size effects. The use of the Grand Canonical Ensemble allows the density for confined and bulk water to be reached as the chemical potential and temperature are imposed. The water/water and water/framework ($AlPO_4$) interactions were modelled with the same interaction potentials as those used in our previous work [14]. In particular, as

described in Ref. [14], some water molecules in $AlPO_4$-54•xH_2O (labelled in this study OW1 and OW2) have low atomic displacements parameters (ADP) suggesting that they are nearly immobile. This result is in agreement with ab-initio calculations in which a few water molecules were found to be framework molecules connected to $AlPO_4$ framework by a short Al-O bond [36]. In the present work, the center of mass of OW1 and OW2 were treated as fixed. For each system, the $AlPO_4$-54•xH_2O structure was allowed to relax using a force field developed for such materials while imposing the experimental cell parameters.

Ab-initio molecular dynamics (AIMD) simulations were performed and the vibrational spectra were extracted from MD trajectories, via the time fourier transform of the velocity-velocity autocorrelation function using the MD trajectories for each atom of the system. The AIMD simulations were performed using CASTEP code (http://accelrys.com/products/datasheets/castep.pdf). Lattice parameters were fixed in the calculation to the values derived at T = 173, 235 and 293 K from previous study [14]. All calculations use optimized ultra-soft pseudopotentials generated with the Perdew-Burke-Ernzerhof (PBE) [37] functional within the generalized-gradient approximation (GGA). We used a plane-wave cut-off energy of 500 eV. Optimized structures were used as input for the production of AIMD trajectories. They were firstly thermal equilibrated at 300 K in the NVT ensemble over 4 ps with a 1.0 fs time step. The equilibration run was followed by a production run of 10 ps, performed also in the NVT ensemble at T = 173, 235 and 293 K. The density of states (DOS) was then computed as time fourier transform of the velocity autocorrelation function (VACF) computed from the coordinates of each step of the trajectories, as implemented in the nMOLDYN program [38]. Details on ab-initio Molecular Dynamics (AIMD) simulations are described in the Supporting Information (SI-section 1).

3. Results and Discussion

3.1 Single crystal synchrotron X-ray diffraction (SC-XRD)

The structure of $AlPO_4$-54•*x*H_2O was refined at *T* = 135, 100 and 50 K using the structural model obtained by previous XRD measurements at 173 K (space group $P6_3$) [14]. As in the previous study, introduction of twinning on the (100) face in the refinement reduced the *R* factor. The final *R* factors (see def. at Section 2 on SI) and structural data (fractional atomic coordinates, atomic displacement parameters (ADP), bond lengths and angles) are given in Tables S1-S5 in the Supporting Information (SI-section 2).

For all temperatures studied, a few water molecules (labelled OW1 and OW2) have low ADP's similar to that for the atoms of $AlPO_4$ framework as they are coordinated to ^{VI}Al (Table S2), as already observed at higher temperature [14,17]. These molecules are in such a strong interaction with the $AlPO_4$ framework that they are nearly immobile [14], in agreement with *ab initio* calculations in which a few water molecules were found to be framework molecules as they are connected to $AlPO_4$ by a short Al-O bond [36]. Upon cooling, the water molecules located at the pore vicinity region (OW3, OW4, OW6 and OW8, see SI-Tables S2 and S3), here termed as *proximal water*, presented ADPs two to three times larger than those of O atoms belonging to the $AlPO_4$ structure. In the pore vicinity sites, water molecules form hydrogen bonds (HB) with the O atoms of the water molecules located at the 6-fold Al.

Figure 1-*top* shows the refined structures of $AlPO_4$-54•*x*H_2O at *T* = 135, 100, and 50 K illustrating the AlO_4 and PO_4 tetrahedra and the positions of the O atoms of water (circle size represents the water O ADP at 50% probability). The simulated structures, Fig. 1-*bottom*, correspond to simulated density maps of the O atoms of water. Upon decreasing the temperature with respect to the previous study limited to 173 K[14], both the experimental (at *T* = 135, 100 and 50 K) and simulated (at *T* = 173, 110 and 10 K) structures show an increase in water ordering and site occupancies at the pore wall. The O atoms of water in the vicinity of the surface exhibit similar ADP to those of the O atoms in ice [39], whereas the ADP values increase towards the pore center. The higher ADP values (experimental) and densities (simulated) observed for inner water at all studied temperatures are representative of a more

disordered arrangement if compared to proximal water. The bridging angles do not change significantly upon cooling (Table S5), which is in agreement with the observation of no major change in the *a* and *c* lattice parameters with *T* (Table S1).

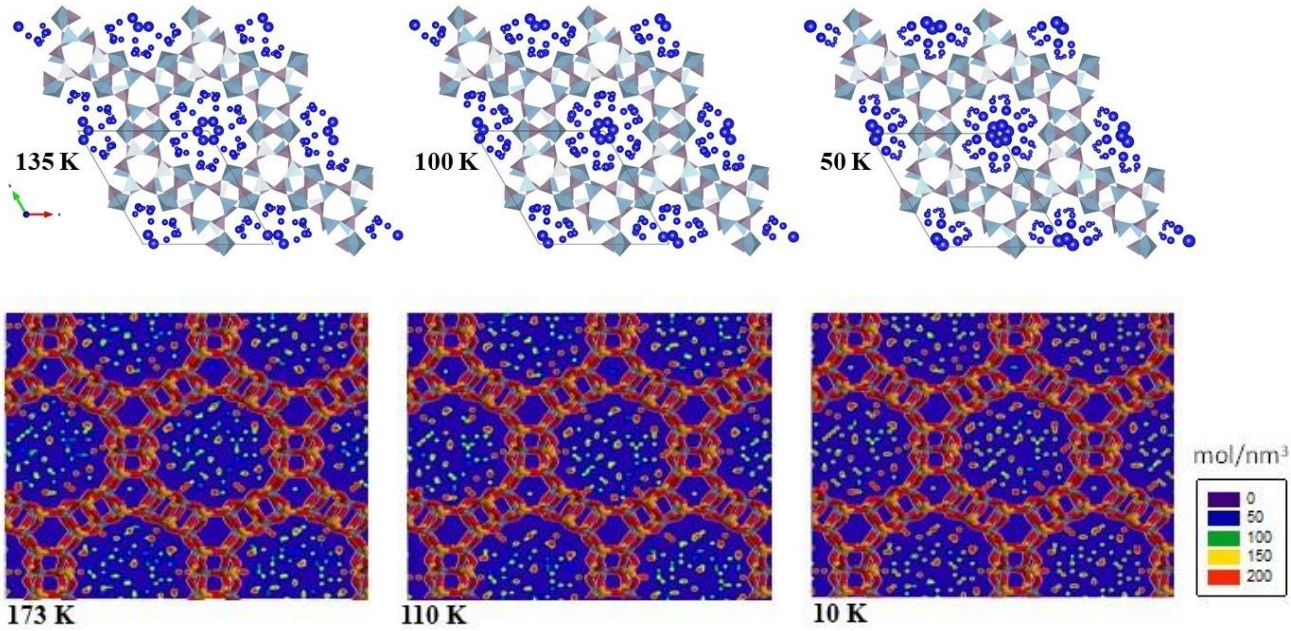

Figure 1: Experimental structure (*top*) and unit cell (outlined in black) of $AlPO_4$-54•*x*H_2O at *T* = 135, 100 and 50 K, obtained from single-crystal XRD. In the experimental data, the light-blue and purple polyhedra are the AlO_4, AlO_6 and PO_4 units of $AlPO_4$ while the dark-blue circles indicate the O atoms of water molecules (the O ADP are represented at 50% probability). Simulated structures (*bottom*) of water in $AlPO_4$-54•*x*H_2O at *T* = 173, 110 and 10 K. These simulated data are density maps of water in $AlPO_4$-54•*x*H_2O. The density scale increases linearly from purple, blue, green, yellow, orange, and red. Note a higher ADP and lower density from *inner water* compared to *proximal water* for all studied *T* in both experiments and simulations.

3.2 Pair-Distribution Function from powder neutron scattering

Pair-distribution function – PDF(*r*) – data obtained from neutron scattering on $AlPO_4$-54•*x*H_2O provides information on the local structure of nanoconfined water upon cooling. At low temperature, the PDF(*r*) features tend to become narrower and of higher amplitude due to the lower Debye-Waller factors (*DW*). However, significant changes in peak intensity and position should reflect structural changes. Fig. 2 shows the pair distribution functions PDF(*r*) of $AlPO_4$-54•*x*H_2O at *T* = 10, 100, 173 and 300 K, and its dehydrated phase ($AlPO_4$-54) at *T* = 10 K. Both the data for the hydrated and dehydrated phase were normalised to the total sample mass illuminated by the beam. Assignment of the peaks can be obtained by comparison with single-crystal XRD data from previous studies [14,17]. The distances above 4 Å are somewhat more difficult to assign, due to the overlap of several features, here we present only the shorter distances region (< 4 Å). At 1.51 Å, 1.76 Å, 1.8-2.0 Å, 2.5 Å and 2.8 Å typical framework intrapolyhedral distances from P–O, Al–O (tetrahedra), Al–O (octahedra), respectively, are found. The inter-tetrahedral Al–P distance across the bridging angle is observed at 3.11 Å. Above 3.4 Å several inter-tetrahedral distances are observed and overlapped, such as O–O, P–O and Al–O. The peak at 2.14 Å is attributed to the Al–H distances involving the 6-fold Al. At 1.82 Å and 2.8 Å the hydrogen bond (HB) and O–O distances from the pore water, respectively, are observed. The peak at 1.18 Å is attributed to a residual amount of adsorbed N_2 [40] from the cryostat atmosphere at the zeolite surface. The PDF(*r*) of $AlPO_4$-54•*x*H_2O shows changes in the $AlPO_4$ structure as temperature decreases. Here we will focus on changes concerning nanoconfined water. Upon cooling, there is a clear sharpening of several peaks in the PDF(*r*), and an increase in the number of O atoms bonded via H-bonds with a typical distance of 2.8 Å, Fig. 2.

For the sake of clarity, we subtracted from the PDF(*r*) of $AlPO_4$-54•*x*H_2O at *T* = 10, 100, 173 and 300 K its dehydrated phase at *T* = 10 K, the result is shown in Fig. 3-*a*. From the PDF(*r*) difference, we observe that, upon decreasing the temperature, the HB (at around 1.82 Å) shifts towards lower values, which is consistent with a strengthening of the H-bond network. As aforementioned, in the $AlPO_4$-54•*x*H_2O structure, one-third of the aluminium cations are octahedrally coordinated due to the presence of two H_2O molecules in their coordination sphere, one of which forms strong hydrogen bonds with the

free water in the pore, while, at 300 K, no hydrogen bonds are formed with the second coordinated water [41]. Figs. 2 and 3-*a* show the shift and a sharpening of the peak at 2.14 Å for temperatures lower than 173 K. Such a shift indicates changes in the local structure of the octahedral environment of Al. Concerning the Al-H intra-octahedral distance (Al-O-H), the slight increase in the peak intensity and the shortening of Al-H intra-octahedral distance (Al-O-H) suggest structural changes in the Al-H environment. In Fig. 3-*b* the simulated PDF(*r*), obtained by MD calculations, is shown for each temperature *T*, where PDF(*r*) = $PDF_{T}(r) - PDF_{T=290\,K}(r)$, for *T* = 110, 173, 218, 233, 258 and 278 K. The simulated data evidence two strong peaks at around 1.82 and 2.8 Å at the lowest *T* (10 K), in agreement with the experiment, indicating an average strengthening of the H-bond together with a structuring of confined water on cooling.

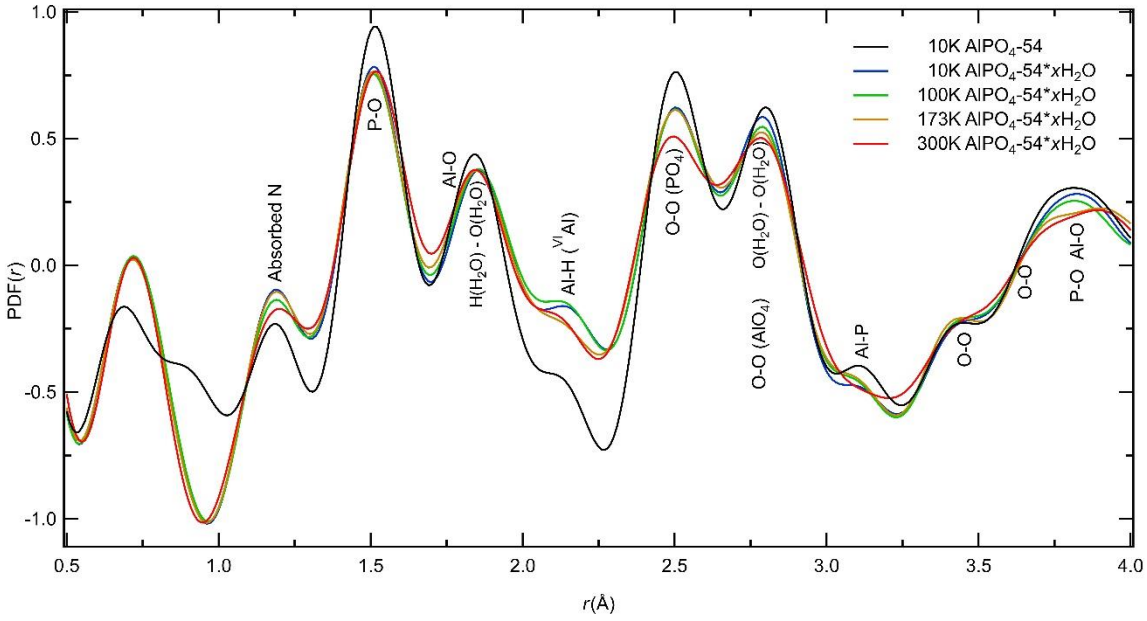

Figure 2: Pair distribution functions PDF(*r*) of $AlPO_4$-54•*x*H_2O at *T* = 300, 173, 100 and 10 K, and for $AlPO_4$-54 at *T* = 10 K.

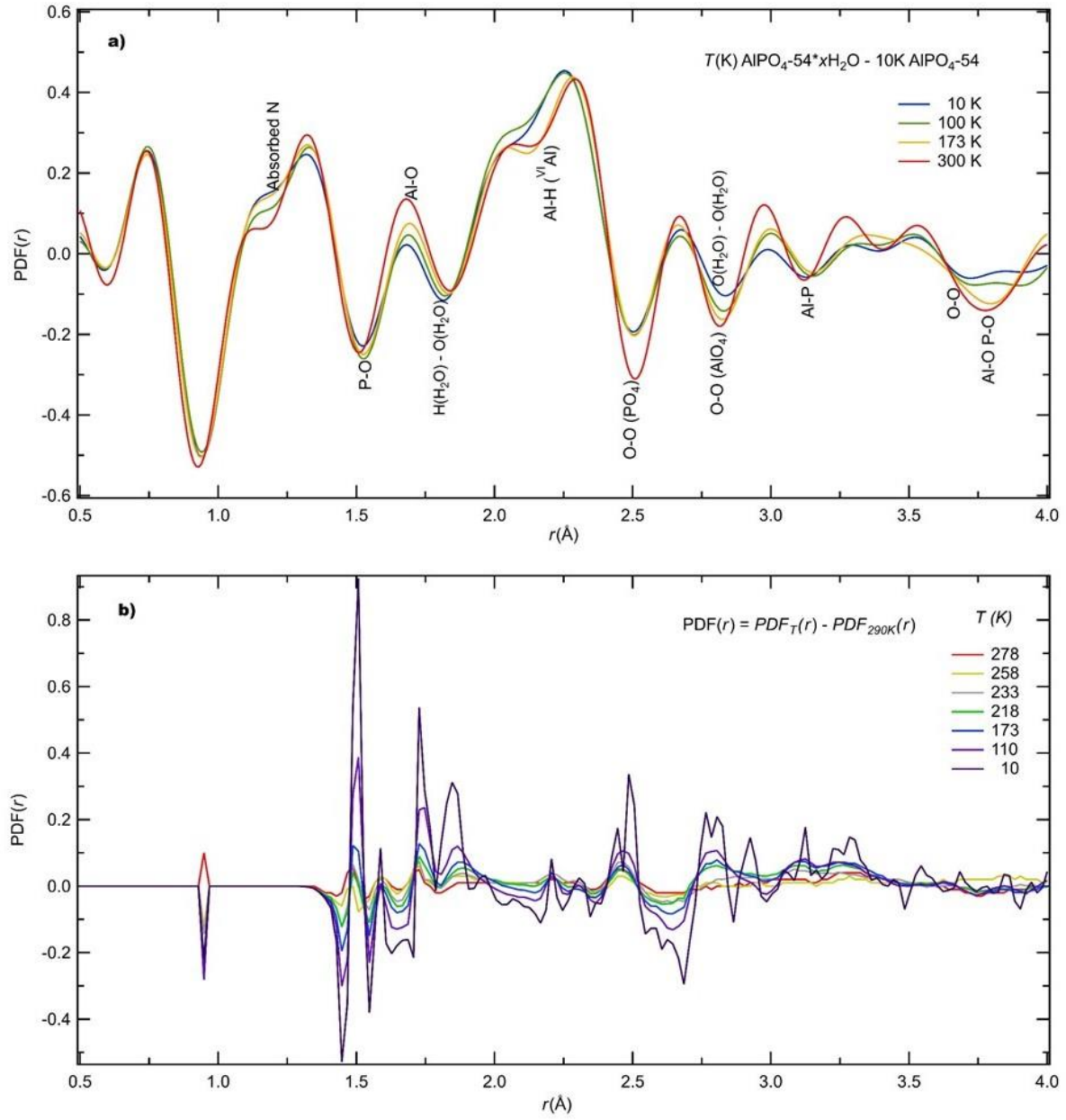

Figure 3: Experimental (*a*) and simulated (*b*) difference of pair distribution functions PDF(*r*) between $AlPO_4$-54•*x*H_2O at *T* = 300, 173, 100 and 10 K and its dehydrated form ($AlPO_4$-54) at *T* = 10 K, for the experimental data. For the simulated data (MD calculations), for each temperature *T*, the simulated data show $PDF(r) = PDF_T(r) - PDF_{T=290\,K}(r)$.

3.3 GCMC simulations – Radial distribution functions and the Hydrogen bonding

GCMC simulations were used to assess the arrangement of water molecules confined in $AlPO_4$-54•xH_2O at different temperatures. Figure 4 shows various simulated pair distributions functions $g(r)$ for bulk (Figs. 4-a and -d) and confined water (Figs. 4-b, -c, -e and -f) at T = 10, 110, 173, 218, 233, 258 and 278 K. Different contributions to the total pair distribution function are shown as they allow the structure of confined water to be identified. In particular, these contributions were chosen to unravel the hydrogen bonding between water molecules (water/water) and between water molecules and the host zeolite (water/$AlPO_4$). As in the case of bulk water, confined water forms a hydrogen bond network between water molecules which becomes more ordered upon decreasing the temperature T (i.e. with correlation peaks in the $g(r)$ functions that have an amplitude/width ratio that increases with decreasing T); these hydrogen bonds correspond to the strong peak at about r~1.9 Å whose amplitude increases with decreasing T (Figs. 4-d and -e). Interestingly, the proximal water also forms a pseudo-hydrogen bonded network with the O atoms of the zeolite as evidenced by the peak – located at a similar distance – in the $g(r)$ between the H atoms of water and the O atoms of the $AlPO_4$-54 structure, Fig. 4-f. However, this peak is less pronounced than that between water molecules (Fig. 4-e), therefore suggesting that ordering in confined water remains mostly driven by water-water interactions (despite the strong hydrophilicity of the zeolite structure). In this respect, it should be noted that direct quantitative comparison between the water/zeolite and water/water correlation peaks cannot be established. However, their integral relates to the number of neighboring O atoms (either from the zeolite or from other water molecules) so that these peaks do reflect the role of specific intermolecular interactions in the structuring of confined water. A strong peak is observed at r~2.7 Å, Fig. 4-b. This peak arises from the fixed O_w, as previous commented, i.e. from the water linked to one-third of the aluminium cations, which are octahedrally coordinated due to the presence of two H_2O molecules in their coordination sphere. Following previous studies [14], these O_w were set at their crystallographic positions. All $g(r)$ functions for T down to 110 K suggests that inner water remains amorphous-like as no long-range positional ordering is observed. In contrast, for T = 10 K, the $g(r)$ functions for confined water suggests that water exhibits *high positional order*, Figs. 4-b, -c, -e and -f. In particular, the $g(r)$ function between

the O atoms of proximal water and those of the zeolite present subpeaks and peaks beyond the first peak corresponding to hydrogen bonding, Fig. 4-c. This result suggests that proximal water might form a more ordered arrangement as temperatures are lowered below T = 110 K, in simulation runs. However, this result, should be taken with caution. From an experimental point of view, it cannot be excluded that kinetics at such low temperatures (typically, T~10 K) are too slow and hinders the formation of ordered water under confinement. In this respect, we note that Monte Carlo simulations might be less prone to such issues because they rely on a sampling of the phase space using Boltzmann factors and not according to a time trajectory as in molecular dynamics simulations (even though sampling in Monte Carlo simulations is also strongly limited by low acceptance probabilities at very low temperatures). However, water dynamics has been observed to be active down to very low temperature under extreme confinement [42], resulting in a water ordering temperature to be strongly reduced.

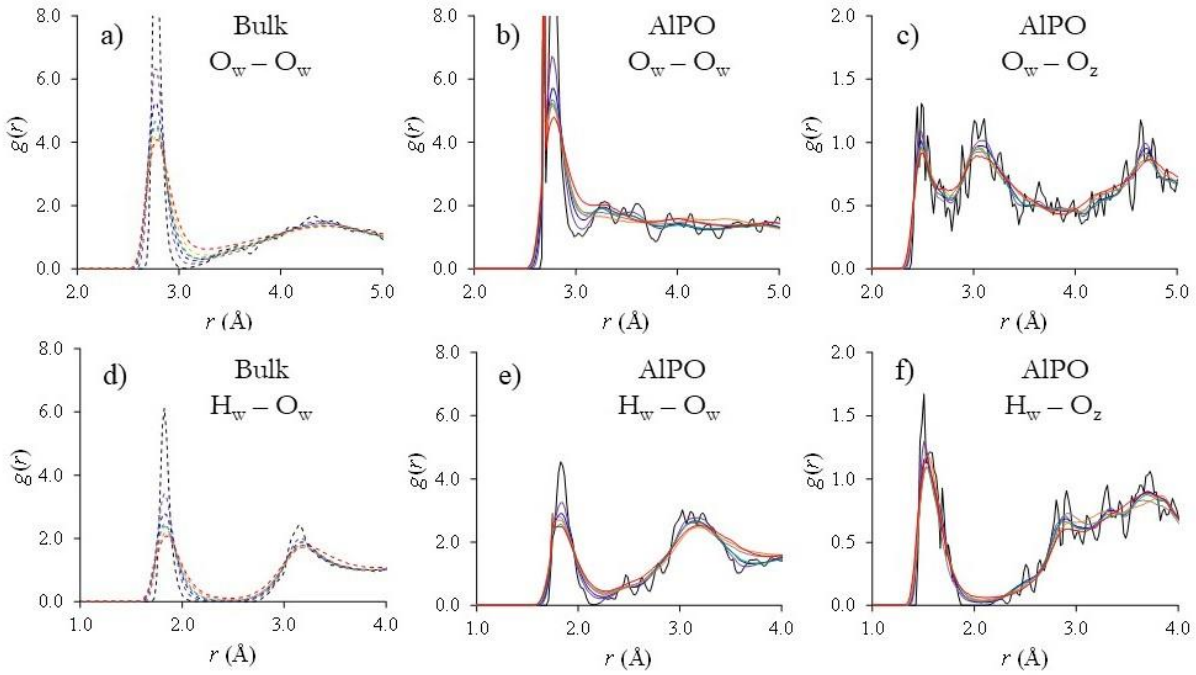

Figure 4: Pair distribution functions $g(r)$ as obtained from Grand Canonical Monte Carlo simulations for bulk water and water confined in $AlPO_4$-54•xH_2O at different temperatures: T = 10 (black), 110 (purple), 173 (blue), 218 (green), 233 (grey), 258 (orange), and 278 K (red). Different contributions to the total pair distribution function are shown (from top, left to bottom, right): $O_w - O_w$ for bulk water, $O_w - O_w$ for confined water, $O_w - O_z$ for confined water, $H_w - O_w$ for bulk water, $H_w - O_w$ for confined water, $H_w - O_z$ for confined water where O_w, O_z and H_w denote the O atom of water, O atom of the zeolite and the H atom of water, respectively.

The pair distribution functions $g(r)$ for confined water (Fig. 4-b) show a sub peak at around 3.2 Å for all studied T. This peak has been identified as the signature of HDA/HDW (high-density amorphous ice) by the TIP4P Ice model [43] and for water under pressure. Compared to the bulk, g(r) for confined water, Fig. 4-b, indicates a much more disordered state, which is not tetrahedral and collapsed. Fixing the 1st shell limit to that of bulk water (3 Å), no vanishing of the g(r) is observed at this value and an excess density of molecules is found between the two next minima 3 and 3.6 Å (red curve). The number of first neighbours for water molecules and the angle distribution between molecules in the first and second shell of neighbours were calculated (section 3 from the SI). Note that a much smaller average number

of molecules for confined water, compared to bulk, is observed in the first shell (Fig. SI-1), as previously observed. This coordination number for confined water depends on the local pore curvature (as flat surfaces or surfaces with curvature of the opposite sign can lead to increased coordination numbers). The hydrogen orientation distribution $P(\theta)$ for confined water (Fig. SI-2) shows angles much more distorted and distributed, as well as a broad peak around 75° and not at 65° like in HDA. Note that this does not correspond to interstitial water molecules and can therefore be identified with the second neighbors. The hydrogen orientation distribution (Fig. SI-2) indicates a loss of tetrahedrality (two peaks at 45° and 75°) and a broader angle distribution and distortion. The results suggest that inner water is even more distorted than a HDA network. This is in agreement with what observed in experiments, as discussed in the following.

To further assess the structure of confined water, Fig. 5 shows distribution of hydrogen bonding angles for water confined in $AlPO_4$-54•$x$$H_2O$ nanopores at different temperatures. Both hydrogen bonding between confined water molecules and hydrogen bonding between confined water molecules (proximal water) and the O atoms of the host zeolite ($AlPO_4$ framework) are shown. These data confirm that confined water at T = 10 K is more ordered as a sharp peak is observed in these distributions together with a secondary peak (in contrast, water confined at higher temperatures does not exhibit this second peak and the distribution is much broader than for T = 10 K). For all temperatures, the main peak is located at an angle ~175° which is very close to the value observed for bulk water. As in the case of the $g(r)$ functions, the orientational ordering of confined water is mostly driven by the water-water interactions as the peak in the angle distribution for water-water hydrogen bonding is more pronounced than that corresponding to proximal water-zeolite hydrogen bonding (water/$AlPO_4$).

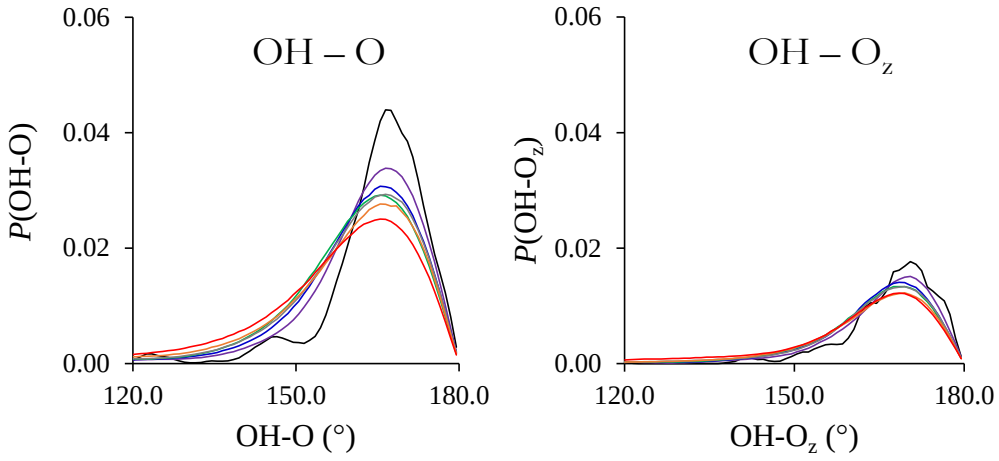

Figure 5: Distribution function of hydrogen bonding angles as obtained from Grand Canonical Monte Carlo simulations for water confined in $AlPO_4$-54•$x$$H_2O$ nanopores at different temperatures: T = 10 (black), 110 (purple), 173 (blue), 218 (green), 233 (grey), 258 (orange), and 278 K (red). The left figure corresponds to hydrogen bonding between confined water molecules (inner and proximal). The right figure corresponds to hydrogen bonding between proximal water molecules and the O atoms of the host zeolite. These histograms are not normalized as the number of molecules $P(\theta)d\theta$ is proportional to the number of H_2O molecules linked to a O_w (left) or O_z (right) atom with an angle between θ and $\theta + d\theta$. Therefore, the marked amplitude difference between the left and right panels indicates that there are more H_2O molecules linked to a O_w (i.e. another water molecule) than to a O_z (i.e. the zeolite framework).

3.4 INS probe the generalised density of states of water confined at the nanoscale

The $AlPO_4$-54•*x*H_2O water vibrational spectrum consists of four main bands: the connectivity band (85-150 cm^{-1}), the librational band (300-1200 cm^{-1}), the bending band (around 1629 cm^{-1}) and the stretching band (2500-3900 cm^{-1}). Bands assignments for the $AlPO_4$-54•*x*H_2O zeolitc water is given in Table 1 [14,15,21,44,45]. The different spectral regions are experimentally studied with different techniques and will be discussed in the current and next section. In particular, the connectivity band and O–H stretching were investigated by IR and will be presented in the 3.6.

Incoherent neutron scattering is a unique probe of individual motions and vibration properties of hydrogen, due to its high incoherent cross section, typically 2 orders of magnitude larger than in other elements [46]. Since vibrations involving hydrogen dominate the incoherent inelastic neutron scattering spectrum, INS can selectively probe the vibrational dynamics of water nanoconfined in zeolite porous and other minerals. Meanwhile, the contribution coming from the framework of the host material should also be considered. The crystal structure of hydrated $AlPO_4$-54•*x*H_2O at ambient, where x = 2.14 [20], counts 38.52 H_2O molecules per unit cell [$Al_{18}P_{18}O_{72}$•38.52H_2O]. Consequently, the total coherent and incoherent cross sections per unit cell for a hydrated $AlPO_4$-54•*x*H_2O are Σ_{coh}≈689.5 barn and Σ_{inch}≈6183.6 barn, respectively. The contribution to the total intensity coming from the zeolitic framework is therefore mainly incoherent due to the two H_2O molecules in the Al octahedra. For a sample with structural water only (x = 0.67, no H_2O in the pore), corresponding to 12.06 H_2O molecules per unit cell, the total cross sections are to Σ_{coh}≈484.55 barn and Σ_{inch}≈1936.17 barn. On the other hand, for a dehydrated material, the number of H_2O molecules per unit cell drops to 4.5 and 2.16, respectively for a sample exposed to primary and secondary vacuum [19]. This gives rise to total cross sections per unit cell for a sample exposed to primary vacuum of Σ_{coh}≈425.99 barn and Σ_{inch}≈722.64 barn, and Σ_{coh}≈407.87 barn and Σ_{inch}≈347.02 barn for a sample exposed to secondary vacuum. Fig. 6-*a* shows a comparison between the INS spectrum of the $AlPO_4$-54•*x*H_2O from 172 to 3900 cm^{-1} at T = 10, 173, 235 and 293 K and its respective dehydrated phase ($AlPO_4$-54) at T = 10 K. The comparison shows that the contribution coming from the zeolitic framework is very low, representative of a structure with fewer

H_2O molecules in the Al octahedra. As will be discussed in the next sections, and already reported in the SC-XRD results, the zeolitic framework does not show significant changes on cooling.

Table 1: Band assignments for $AlPO_4$-54•xH_2O zeolitc water at ambient pressure and temperature [14,15,21,44,45].

Wavenumber (cm^{-1})	Assignment	Label
3559	O–H Stretch trimers, dimers, monomers	ν_{OH3}
3345	O–H Stretch intermediate coordination	ν_{OH2}
3149	O–H Stretch tetrahedral H bonds	ν_{OH1}
1628	HOH Bending	HOH
940	Librational *axe x - wagging*	ω_3
737	Librational *axe z - twisting*	ω_2
545	Librational *axe y - rocking*	ω_1
126	Connectivity H-bond	νHB_3
116	Connectivity H-bond	νHB_2
109	Connectivity H-bond	νHB_1

From the INS spectra from $AlPO_4$-54•xH_2O (Fig. 6-*a*), three main regions typical of specific water vibrational modes can be distinguished. In the region from 300 to 1200 cm^{-1} intermolecular librational modes (frustrated rotational oscillations) are present. Around ~1628 cm^{-1} the HOH bending mode is visible. At higher energies, from 2500 to 4000 cm^{-1} the vibrational modes are assigned to OH stretching. The stretching bands are poorly measured on an inverse geometry spectrometer (as LAGRANGE), due to the presence at high energies of a high Debye-Waller factor (even at low temperatures). For this reason, the OH band is overdamped and in addition shows multi-phonons contributions [32,33,47]. Conversely, the $AlPO_4$-54•xH_2O INS spectrum shows a well visible band in the region (300-1200 cm^{-1}), which corresponds to the librational bands of water molecules and which is not probed by other spectroscopic techniques (such as Raman and IR), as this region is typically dominated by the zeolite framework modes. Since the highest energy-part of the INS spectra (> 2000 cm^{-1}) did not show significant features, and can be better probed with other spectroscopic techniques, we focus the present

analysis mainly in the region from 250 to 1250 cm^{-1} (31-156 meV), with further comments on the bending mode, located at 1628 cm^{-1}.

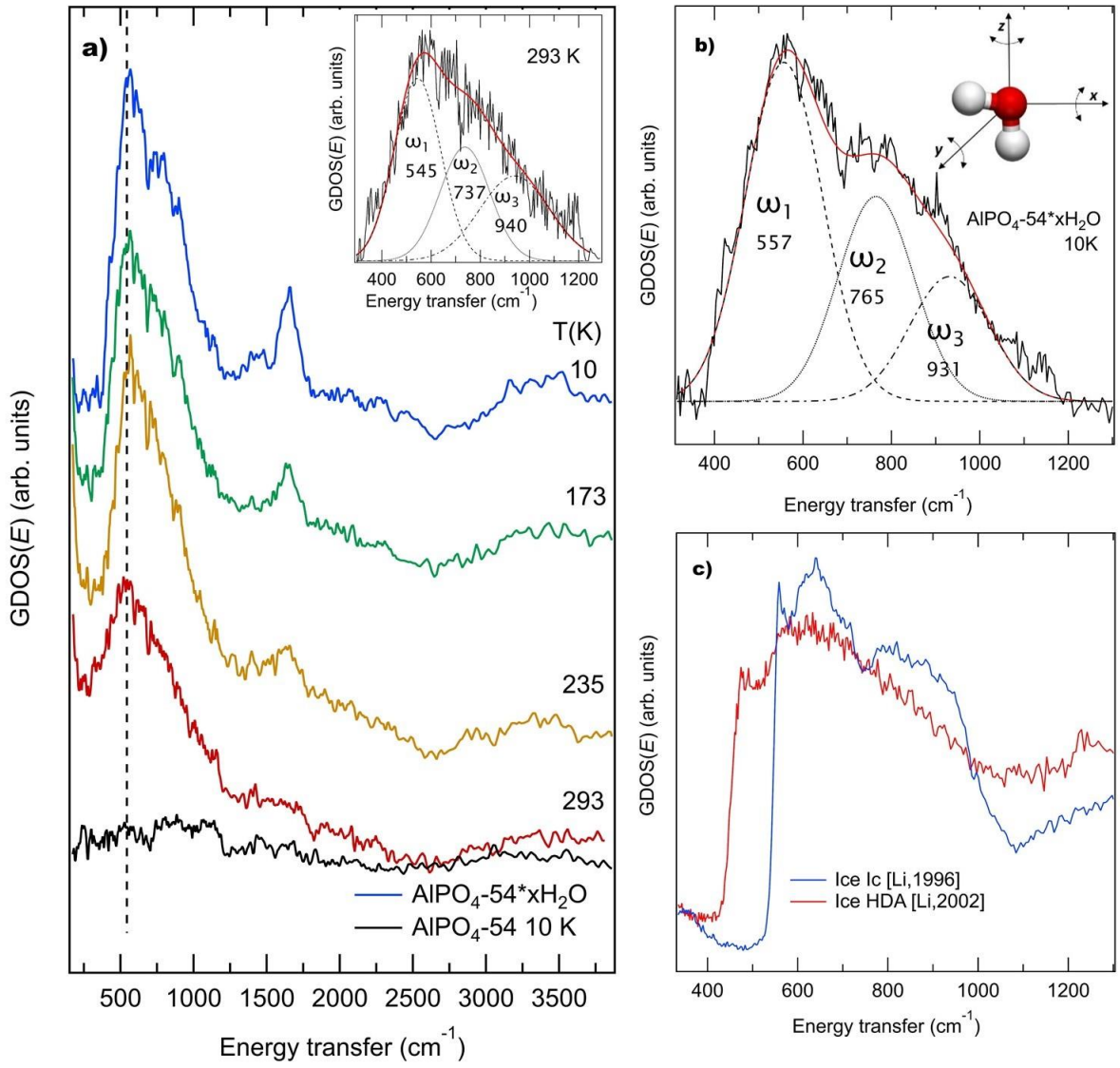

Figure 6: (*a*) INS spectra of $AlPO_4$-54•*x*H_2O (coloured) at *T* = 10, 173, 235 and 293 K and dehydrated (black) $AlPO_4$-54 at *T* = 10 K. Inset-*a*: librational band for $AlPO_4$-54•*x*H_2O at *T* = 293 K together with the deconvoluted Gaussian components (dashed lines) corresponding to the three librational modes around the three symmetry axes of water molecules (see inset-*b*; H white sphere, O red sphere). (*b*) INS spectra of $AlPO_4$-54•*x*H_2O at *T* = 10 K together with the deconvoluted Gaussian components (dashed

lines). (*c*) Normalized INS spectra comparison between ice Ic (blue line) and high-density amorphous ice (HDA, red line), reproduced from Refs. [48,49].

The librational motions of water about the three principal axes of an isolated molecule are referred to as the wagging, twisting and rocking vibrations respectively, with only two of these being IR and Raman active. In contrast, the three libration modes are observed by neutron scattering. The three symmetry axes are defined as: the *y* and *z* axis are the molecule plane; while the *x* axis is perpendicular to the plane (Fig. 6-*b*, inset). The observed sub-bands ω_1, ω_2 and ω_3, Fig. 6-*a inset*, correspond to the librational modes around the axes *y*, *z*, and *x*, respectively [44,50].

Hydrogen bonds of nanoconfined water are expected to become stronger with decreasing temperature. Moreover, changes in the structure of the nanoconfined water should be reflected in the intermolecular vibrational spectra, particularly the librational bands which are very sensitive to variation in H-bond. For the latter, the stronger (and/or more structured) the bond the lower the resulting energy. Consequently, higher frequency intermolecular modes are observed, as in Ice compared to water [51], as a more structured hydrogen bond network produces a stronger restoring force. The dashed vertical line in Fig. 6-*a* is a guide to the eye fixed at the ω_1 sub-band position at T = 293 K. At the lowest temperature (T = 10 K) the INS spectrum shows some changes in the librational band with respect to room temperature: an intensity increase and two better defined maxima are observed (Fig. 6-*a* and -*b*). As in the PDF(*r*), upon cooling the INS spectra are expected to increase in intensity, due to the Debye Waller (*DW*) factor. On the other hand, a more structured librational band is a clear signature of a more ordered structure. In bulk water, the librational band evolves strongly from a broad band in the liquid phase to a sharp and intense structure in hexagonal ice [48]. Here, the observed changes suggest that at low T (10 K) there is an increased contribution from an ordered arrangement with the number of H-bonds increasing to a total average somewhat less than the four per molecule (like ice) [48]. It must be remarked that the spectra of Ic, Ih and LDA ices are almost superimposed in the librational region [48]. Indeed, the crystalline (Ic and Ih) and amorphous ice (LDA) have similar density and a coordination number of about 4, their local structures being basically the same [48]. Conversely, the INS spectrum from the

librational band of the high-density amorphous ice (HDA) [48] strongly differs from those of Ic, Ih and LDA ices (Figs. 6-*c*). HDA shows a general broader band, which starts at lower energy and presents less intense and broader modes at higher energy. Such features in HDA's librational mode are linked to interpenetrated structures, as present in ice VII and VI. Fig. 6-*b* presents the INS spectra of the librational band from $AlPO_4$-54•*x*H_2O at *T* = 10 K, in comparison with Fig. 6-*c* which presents the librational from a crystalline ice Ic and high-density amorphous ice (HDA). The librational band of the zeolitic nanoconfined water at the lowest *T* (10 K) shows common features with both bulk ices, though overall the modes are slightly shifted to lower frequencies. Indeed, it presents two *sharp* maxima similar to those observed in ice Ic spectrum, and similarly to HDA a broad high frequency mode (ω_3) at frequencies of about 900-1000 cm^{-1}. And similar to the HDA, a structure extending at lower frequencies with a shoulder at around 474 cm^{-1}. This observation supports once again the hypothesis that at the lowest *T* the arrangement of nanoconfined water molecules may be a superposition of a locally ordered arrangement (as indicated by the two well defined maxima), together with a high-density disordered arrangement (as indicated by its broad lower energy contribution). This scenario is in agreement with XRD, GCMC and PDF results.

The INS spectrum also shows evidence for temperature effect on the HOH bending mode. This single component band increases in intensity upon cooling, due to the *DW* factor, and shift to higher frequencies, Fig. 6-*a*, varying from ~1628 cm^{-1} at room temperature (Table I) to ~1686 cm^{-1} at *T* = 10 K. This variation similar to the one observed in bulk water during crystallisation [52] and the non-evolving single Gaussian shape is an indication that the bending mode is not sensitive to the modifications of connectivity of the nanoconfined water.

The INS, mid- and far-IR spectral profiles of the vibrational modes of water confined in the $AlPO_4$-54•*x*H_2O nanopores (connectivity, librational and stretching) can be described by several overlapping Gaussian components after removing the slowly rising linear background [21,45,52,53]. This technique was recently applied successfully to other $AlPO_4$ molecular sieves and zeolites to evidence the correlation between structural and vibrational properties [21,45,53]. A complete description can be found in previous work [21,45,53]. For clarity, we only present the water band region prior to the background removal together

with the fitted Gaussians and their assignment. Such a fit provides a sound tool to quantitatively account for the changes of water modes, although the present Gaussian and background fit is not unique. Fig. 7 shows the temperature dependence of the INS librational sub-bands frequencies and their respective full widths at half maximum (FWHM). The decrease of the librational width, compared to bulk water, is attributable to the ordering arrangements of hydrogen atoms, as observed in ice [54,55]. The librational sub-bands frequency can be roughly correlated with the strength of the hydrogen bonding while the width is inversely related to the robustness of the network. Upon decreasing *T* both lowest energy libration sub-bands (ω_1 and ω_2) are observed to shift to higher wavenumbers while a decrease in the FWHM of the three the modes (Fig. 7) is observed. The shift in frequency is an indication of the formation of a network with stronger HB upon lowering *T*, which is in agreement with the PDF results, while the narrowing suggests more robust bonds. The highest energy mode (ω_3) presents stronger changes: the FWHM strongly decreases with temperature, while its frequency does not show a particular trend. The shift in frequency is an indication of the formation of a network with stronger HB upon lowering *T*, which is in agreement with the PDF results, while the narrowing suggest a more robust bonds.

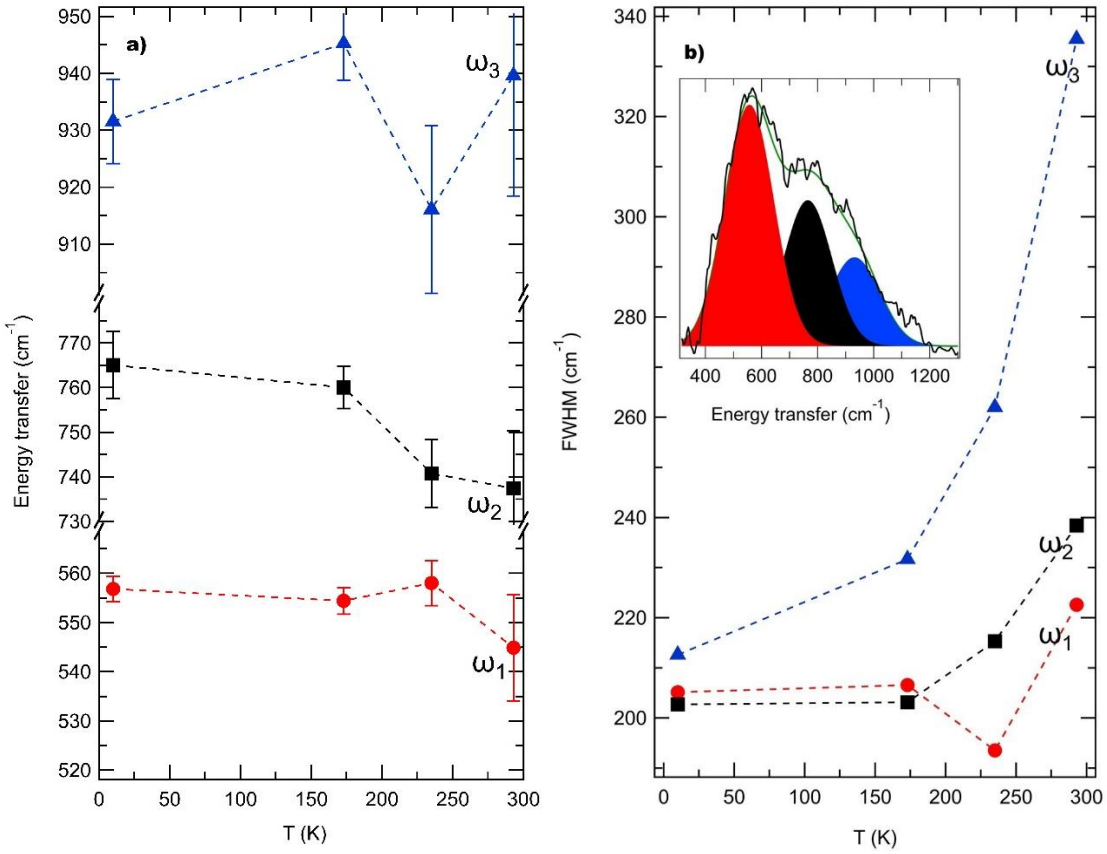

Figure 7: (*a*) Intermolecular librational mode frequencies and (*b*) full width at half maximum (FWHM) of the librational sub-bands at selected temperatures. Inset-*b*: the librational band with the three components at 10 K.

3.5 Ab-initio Molecular Dynamics simulations

Simulations by AIMD were performed for the $AlPO_4$-54•*x*H_2O system to support and better interpret the experimental results. The atomic contributions to the density of state of the H atoms g_H (*E*) are determined for water in various locations. In particular, both structural (linked to ^{VI}Al) and confined (nano unidirectional pore) water, in which only the oxygen atoms from H_2O is considered, were included in the model. The density of states for two types of H have been labelled: those in H_2O coordinated to the ^{VI}Al and those to the nanoconfined pore water, named H-coordinated (structural) and H-pore (inner and proximal), respectively. Fig. 8 shows the comparison of the calculated, $g_{H\text{-coordinated}}$ (*E*) and $g_{H\text{-pore}}$ (*E*), and the total hydrogen vibrational density of states g_H (*E*), of $AlPO_4$-54•*x*H_2O for *T* = 173, 235 and 293 K. Four main bands are observed, as described previously: the connectivity band (85-150 cm^{-1}), the librational band (300-1200 cm^{-1}), the bending band (around 1629 cm^{-1}) and the stretching band (2500-3900 cm^{-1}). Here we will focus on changes concerning the librational band, while further comments on the connectivity and stretching band appear in the next section (IR at low *T*). The dashed vertical line is, here again, a guide to the eye and represents the ω_1 sub-band position from the INS results at *T* = 293 K. AIMD shows that changes on the librational band are dominated by the adsorbed confined water (inner and proximal). A red shift of the librational lower edge, together with a variation in intensity, is observed when decreasing the temperature from *T* = 235 to 173 K. Such a shift and its respective change with temperature in the librational band shape is observed also at the INS spectrum, Fig. 6-*a* and 7, and involves mostly both lowest sub-bands (ω_1 and ω_2, Fig. 7), which shows a good agreement between INS and AIMD. Such a shift (see dashed line guide) and the overall librational intensity change suggest some modification in the nanoconfined water network. In the following, these strong indications of dynamic transitions will be confronted with the IR results.

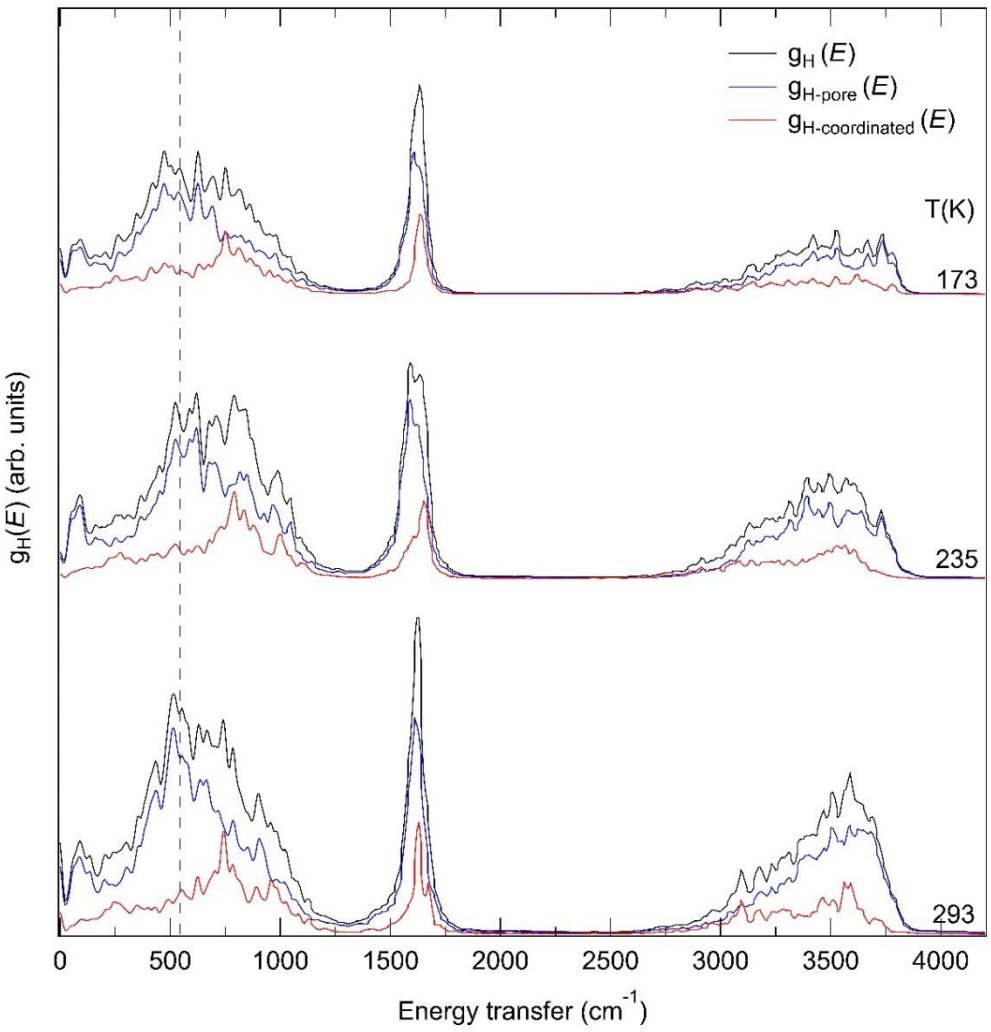

Figure 8: Comparison of the calculated, $g_{H\text{-coordinated}}$ (*E*) and $g_{H\text{-pore}}$ (*E*), with the total hydrogen density of states g_H (*E*), of $AlPO_4$-54•*x*H_2O for *T* = 173, 253 and 293 K.

3.6 Far- and mid-IR absorption at low temperature

Far- and mid-IR spectra of water confined in $AlPO_4$-54•xH_2O nanopores were measured in a wide range of temperatures to complete the water vibrational information obtained from other techniques. The infrared measurements are dominated by contributions from molecules located in the pores, as shown by the g_H (*E*), Fig. 8. Moreover, from the single crystal XRD results (section 3.1) and a previous study [14], the strength of the $AlPO_4$-54•xH_2O structural framework constraints being negligible upon cooling, changes in absorption are representative of the *evolution* of the nanoconfined water. The present IR measurement is only presented between 50 and 150 cm^{-1} and between 2000-4000 cm^{-1}, the intermediate energy range (150-1800 cm^{-1}) being masked by strong modes due to the structural framework. For this reason, the present IR spectra only probes part of the connectivity (H bond stretching) and the O-H intramolecular water vibration.

The OH Stretching band

Fig. 9-*a* shows the IR spectra of nanoconfined water in $AlPO_4$-54•xH_2O in the region of the OH stretching band measured at various temperatures between 300 and 17 K. For all temperatures, this band is extremely wide in energy, covering continuously the range between 2500 and 3700 cm^{-1}. At ambient *T* (*cryogenic T*), $AlPO_4$-54•xH_2O OH presents three broad sub-bands at around 3149, 3345, 3559 cm^{-1} termed νOH_1, νOH_2, νOH_3 and in the following, as well as in Table 1. The dashed vertical line is a guide to the eye and represents the νOH_2 sub-band position at T = 300 K. The contribution of these modes are negligible in the equivalent dehydrated state, as shown by the g_H (*E*), Fig. 8, and by previous studies on $AlPO_4$-54 [21]. Water molecules can establish bonds between confined water molecules (such as inner-inner and/ or proximal-proximal water) and between proximal water and the $AlPO_4$-54•xH_2O framework [45]. In analogy with the measurements by Zanotti et al [56], presented in the insert of Fig. 9–*b*, the first layer of water molecules in direct contact with the hydrophilic surface gives rise to an OH stretching mode around 3150 cm^{-1} (νOH_1) revealing that the H Bonds at play are significantly stronger than in the lowest energy mode in bulk water (liquid or even ice). The other two frequency substructures (νOH_2 and

νOH_3) are therefore assigned to water in interaction with other water molecules in the pores, which can be assigned each to a different population of water molecules with a distinct network, such as for inner and proximal water. These modes appear at very high frequency suggesting that the establishment of hydrogen bond is hindered, likely due to the small size and curvature of the pores. In Fig. 9-*b* and -*c*, the OH stretching of $AlPO_4$-54•xH_2O measured at 17 K is respectively compared with the monoalayer of water measured in porous Vycor, where all four bonds are established, with bulk liquid water, hexagonal (Ih) and low density amorphous ice (LDA). This comparison strongly supports two different water molecules assembly coexisting at the lowest *T*: (i) one layer in direct contact with the pore walls with strong H bonds established giving rise to the shoulder at 3150 cm^{-1} together with (ii) two networks of H bonds, associated to the proximal and inner water populations, respectively absorbing between 3300 cm^{-1} and 3700 cm^{-1} and resembling amorphous ice and liquid water (see comparison Fig 9-*b* and -*c*). These observations of two separate networks co-exiting within the nanopores are clearly in agreement with the deductions from the libration studied by INS, also supported by the SC-XRD results.

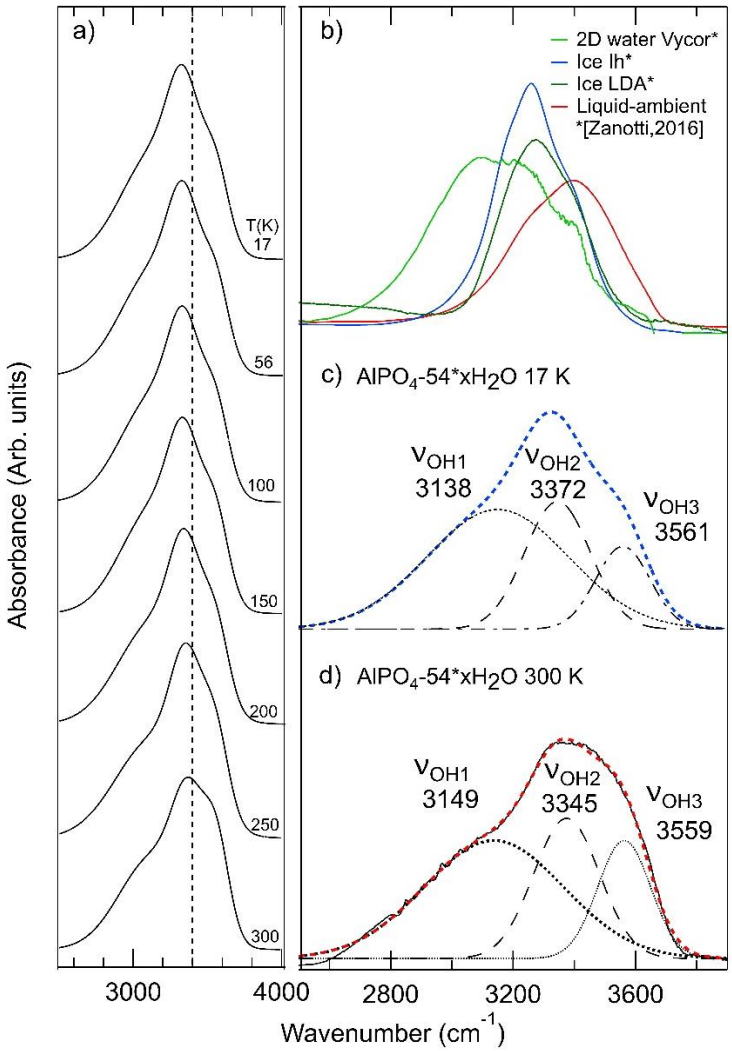

Figure 9: (*a*) OH stretching band of $AlPO_4$-54•*x*H_2O at selected temperatures. (*b*) The spectra of water monolayer in Vycor [56], hexagonal ice (Ih, blue line) [56], low-density amorphous (LDA, green line) [56] and bulk liquid water (red line) are shown for comparison. (All spectra were measured on the AILES beamline). (*c*) and (*d*) OH band of $AlPO_4$-54•*x*H_2O measured at 17 K and 300 K, respectively, with deconvoluted Gaussian components (dashed lines).

The low energy connectivity band

Fig. 10-*a* shows the evolution as a function of *temperature* of part of the connectivity of water in $AlPO_4$-54•*x*H_2O as well as measurement for the dehydrated phase $AlPO_4$-54 at 17 K. As stated previously, the connectivity is possibly extending in a wider range than presented here but the higher energy range is masked by structures from the confining system. At ambient *T* (*cryogenics T*), this low energy band presents three features at around 109, 116 and 126 cm^{-1} termed *v*HB_1, *v*HB_2 and *v*HB_3 in the following, Table 1 and Fig. 10-*c*. These modes are not observed in the equivalent dehydrated state, as shown by its dehydrated spectra, Fig. 10-*a*, and by the g_H (*E*), Fig. 8. The vertical line is a guide to the eye for the *v*HB_2 sub-band position at *T* = 300 K. In agreement with the OH band deductions, we expect two water networks with (i) H bonding established between confined water molecules and (ii) between proximal water and the $AlPO_4$-54•*x*H_2O framework [45]. Based on the g_H (*E*), calculations, Fig. 8, and by comparison with the measurements of water confined in Vycor by Zanotti et al[56] and in zeolites in previous study [45], the HB strong bond between proximal water molecules and the pore surface is expected to give rise to a weak band extending between 120 and 250 cm^{-1}. In the present system, only its lowest frequency part is visible here and may correspond to (*v*HB_3). The lower frequency substructures (*v*HB_2 and *v*HB_1) imply weaker H-bonds and can consequently be assigned to H-bonds from water-water interactions (such as for inner and proximal water). This is in good agreement with the g_H (*E*) calculations for confined water predicting connectivity structures under 100 cm^{-1}.

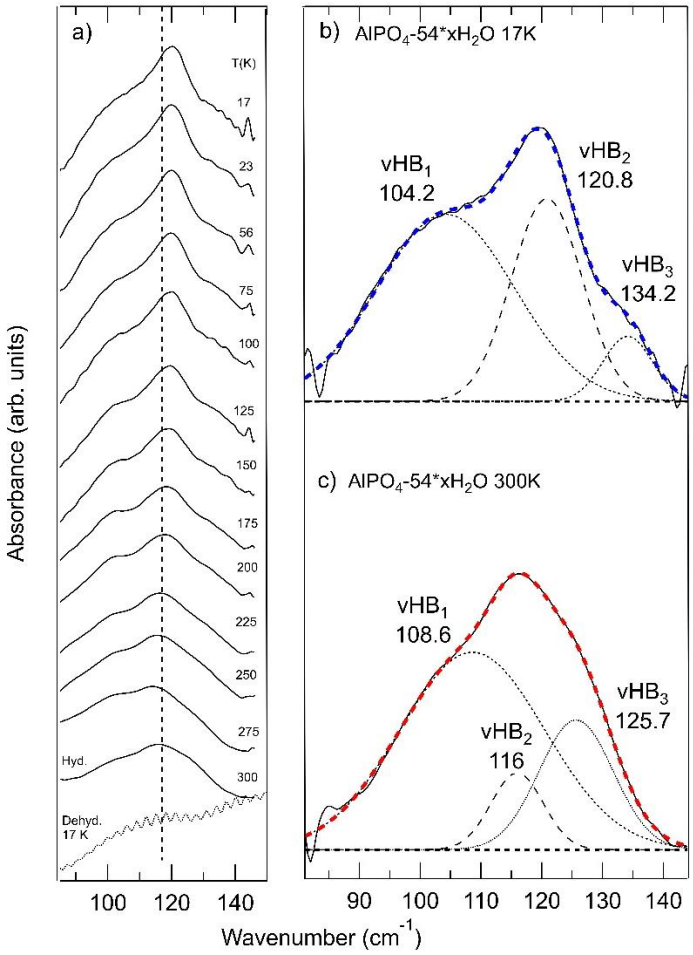

Figure 10: (*a*) Part of the low energy spectra of $AlPO_4$-54•xH_2O at selected temperatures (full line) and the dehydrated $AlPO_4$-54 at 17 K (dot line). (*b*) and (*c*): part of the connectivity band from the difference between hydrated and dehydrated sample measured at 17 K and 300 K with deconvoluted Gaussian components (dashed lines).

A best fit with 3 Gaussians, such as presented Fig. 9-*c/d* and 10-*b/c*, have been realised for both OH and connectivity bands measured at various temperatures. Fig. 11-*a* reports the temperature dependence of the three Gaussian frequencies, with their respective FWHM (Fig. 11-*b*) and, integrated area (Fig. 11-*c*) for the OH stretching, while Fig. 12 presents some equivalent parameters for the connectivity fit.

Changes in the bands evolution are observed at two *temperatures*: around 150 and 250 K. Similar changes on water vibrational modes were observed after cooling down one monolayer of water at the surface of the larger pores of Vycor glass [56], at 160 and 250 K, and for water in the porous silica substrate (MCM-41/C10) with T depending on the applied pressure [10]. In both studies, they were associated with two dynamical transitions, related to modifications of the HB network. A first transition, at around 250 K, can be observed in the lower energy mode νHB_1, Fig. 10-*a*. In the present system, the most visible change in HB bond is observed for the νHB_2 mode, which shows a well-defined maxima starting around 150 K (Fig. 10-*a*).

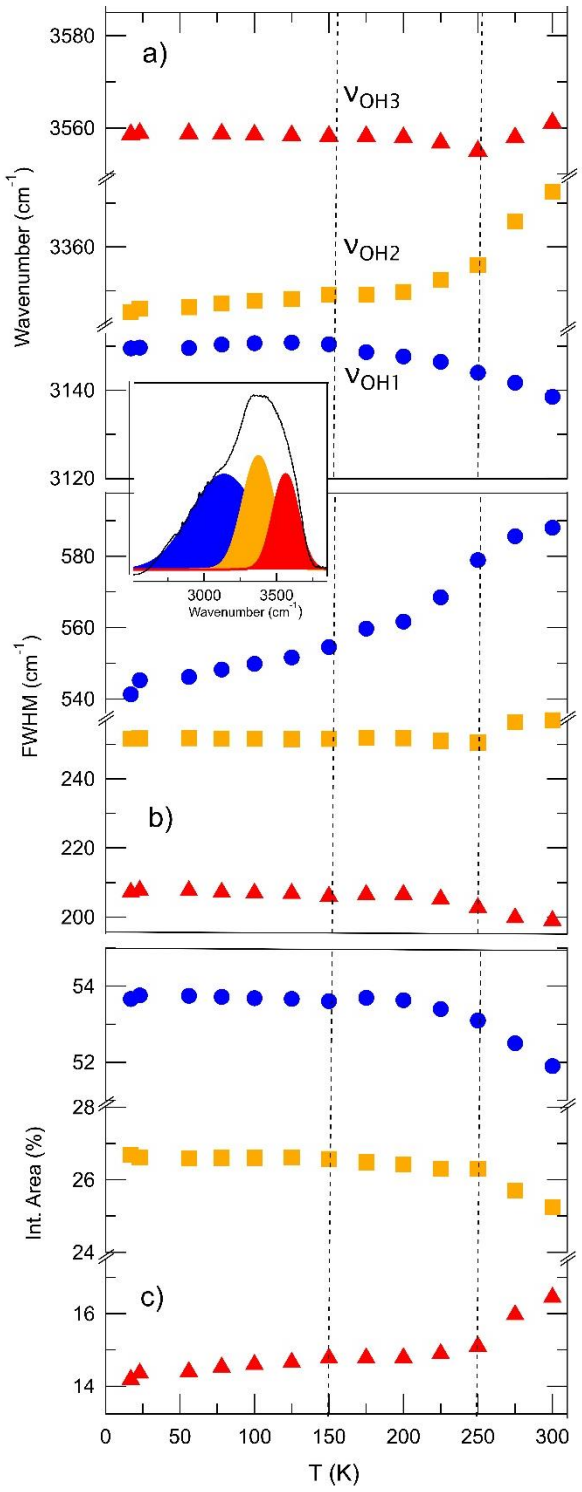

Figure 11: $AlPO_4$-54•xH_2O OH three components modes as a function of temperature (*a*): frequency of νOH_1, νOH_2 and νOH_3 (*b*)*:* full width at half maximum FWHM and (*c*): Integrated area. Errors are smaller than symbol size. Insert: the OH band with the three components at 300 K.

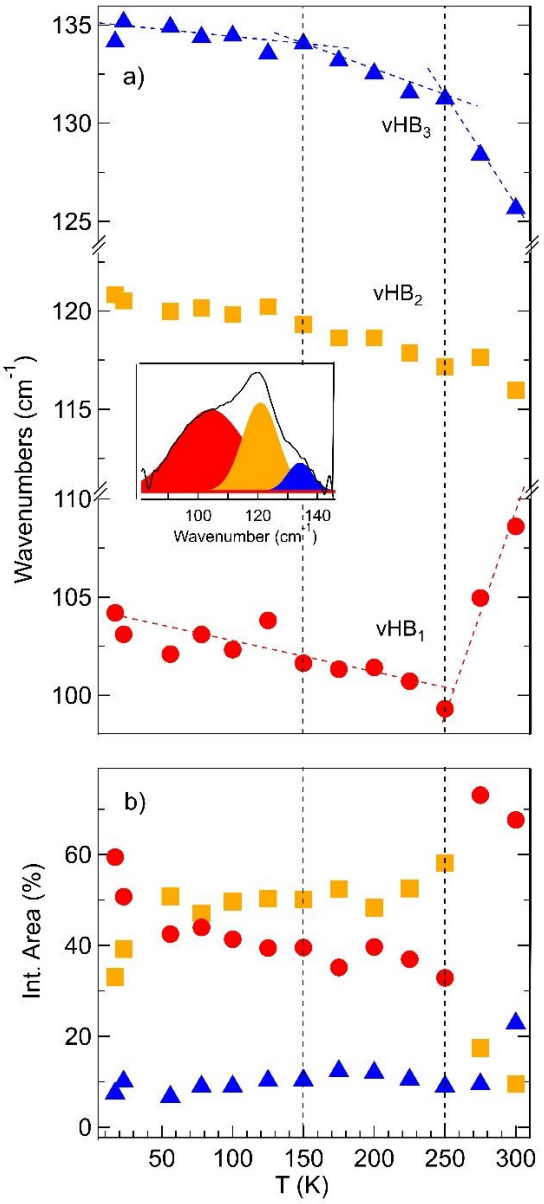

Figure 12: $AlPO_4$-54•xH_2O connectivity three components modes as a function of temperature (*a*): frequency of νHB_1, νHB_2 and νHB_3 (*b*): Integrated area. Errors are smaller than symbols size. Insert: the connectivity band with the three components at 17 K.

(i) From T = 300 to ~250 K (RT). The frequency of the two OH sub-bands νOH_2 and νOH_3, shift abruptly to lower values (see Fig. 11-*a*, -*b*) corresponding to a dynamical transition temperature for both populations of water molecules in the pore. This evolution is clearly associated to inner water evolving to a denser liquid [14,56]. In opposition, ν_{OH1} shifts to higher energies suggesting a continuous increase of the H-bond strength between proximal water and the pore walls, which is confirmed by the evolution of the νHB_3 mode.

(ii) From T = 250 to ~150 K. Both inner and proximal water show changes in their network. The discontinuities evidenced by the HB modes parameters suggest a transition at 250 K, see Fig. 12-*a* and *b*. From 250 K, νOH_2 and νOH_3 (associated to inner water) show changes indicating a less percolative network. The νOH_1 frequency (associated to proximal water) markedly increases while its FWHM decreases coherently with proximal water population evolving toward shorter distances between water molecules and the walls, in agreement with a more ordered network of water molecules. Meanwhile, νOH_2 and νOH_3 show opposite evolution in both intensity and frequency. This latter behavior is associated to the inner water population developing stronger H-bonds as shown by the increasing in frequency of both νHB_1 and νHB_2. The inner population is characterized by a more disordered network, which is glassy-like rather than an ice-like, in agreement with previous study [14].

(iii) From T = 150 to ~17 K. From 150 K, various parameters suggest a transition involving the water network at 150 K, evidenced by shifts in frequency from νOH_1 and νOH_1 modes. From 150 K, the OH stretching frequencies and width remain constant except for the νOH_1 width, which decreases pointing at a decreasing mobility, related to the proximal water. In contrast, the connectivity components, νHB_1 and νHB_2 assigned to inner water become significantly stronger suggesting continuous strengthening of in the inner water network. This may be related to the change of the arrangement of water molecules (see insert of Fig. 12) showing a more compact structure as *T* decreases. The fact that the intensity of the νHB_3 band increases also signing some modification of the water network possibly linked to a change in water density as supported by the denser inner water as observed with PDF and GCMC simulations.

As for bulk water, shifts on the melting temperature are expected and have been experimentally observed [10,57] for water under nano-confinement, due to the Gibbs-Thomson effect [10,58]. However, such a shift depends on several factors, including pore size and pore wall properties [59]. A different behaviour of proximal and inner water populations is here observed in the IR results, similar to what has already been observed for water confined in a silica matrix (MCM system), but at higher temperatures [10]. Here, the smaller pore diameter shifts to lower temperatures the water freezing temperature and the hydrophilicity of the pore surface induces a clear distinct behaviour of the two water populations as far as the diffusive dynamics are frozen. The long range zeolite crystal framework may indeed contribute to the proximal water ordering, acting as a orientational template. This is in agreement with GCMC simulations, which suggests that proximal water might form ordered arrangements at lower *T* close to 110 K. Such a *freezing* in the proximal water network is evidenced by IR at 150 K is consistent with an ordering of the H_2O molecules involved in hydrogen bonding with the structural water linked to the framework, also evidenced by the strong changes observed by PDF in the local structure of the octahedral environment of Al below 173 K.

4. Conclusion

The structure and vibrational properties of water molecules confined in unidirectional hydrophilic nanopores of $AlPO_4$-54•xH_2O were investigated at low temperatures. On cooling, from RT down to ~250 K, two distinct water networks appear: *proximal water* near the pore wall and *inner water* at the pore centre. From 250 down to ~150 K, both proximal and inner water develop more defined local arrangements and with distinct long range order: while proximal water is well ordered at the pore wall due to strong interactions with the pore surface [14], inner water retains a disordered arrangement with a glassy-like behaviour (for inner water, ordering is hindered as the pore curvature prevents the formation of a network of tetrahedrally coordinated molecules [14]). From ~150 down to ~10 K, our new results point to a strengthening of the water-water interactions.

While proximal water shows continuous increasing in its ordering upon cooling, inner water becomes more disordered and thus the distinction between the two networks increases. Such ordering for proximal water may be driven by water-water interactions despite the strong hydrophilicity of the zeolite structure. The formation of a more highly ordered local arrangement on cooling below ~150 K is evidenced by IR measurements for proximal water, evidenced by its modes evolution on both OH stretching and connectivity bond. Such a more ordered arrangement is also confirmed by the PDF results and GCMC simulations which indicate a hydrophilic bond of proximal water with the host matrix. INS results suggest an increasing mix of denser amorphous and lighter (less dense) ordered arrangement in water confined down to the lower T (10 K). The librational band presents defined features arising from a lighter ordered local structure (such as Ic and/or LDA ices), embedded in a broader band arising from a disordered denser state. Both experiments and simulations results suggest an overall *densification effect* on cooling. The calculated PDF(r) shows an increased numbers of water molecules held at van der Waals distances (≈ 3.3 Å), in line with a denser state, such as HDA. Such a population of water molecules is disordered and the presence of interstitial molecules could explain the presence of stronger, i.e., shorter HB [43]. Simulations, far-IR and INS results suggest that inner water is even more distorted than HDA, but similarly denser. Moreover, since the framework is essentially rigid (XRD results shows no variation on the pore size), the overall density of water must be constant. In this line, the densification

can only occur for the inner water, whereas the density of the proximal water must decrease to keep the overall density constant.

In conclusion the low *T* experiments suggests the presence of two distinct unidirectional arrangement of water molecules in the $AlPO_4$-54•xH_2O nano-channels, whose coexistence persists at the lowest studied *T*. Upon cooling below 150 K a dense arrangement of water molecules with a degree of orientational disorder even greater than HDA and a glassy-like behavior develops and is embedded in a less dense and highly ordered local arrangement of water molecules, whose orientational order is mainly dictated by the pore surface. These two independent networks imply very diverse settings: one supporting mobile water with many free H-bonds located in the center of the pores (inner water) while the other one is strongly bonded to both the interface and other water molecules (proximal water) and acts as amorphous 2D ice with very low reactivity.

Corresponding Authors

*Frederico G. Alabarse, present address E: frederico.alabarse@elettra.eu ; T: +39.337.127.0679 ; Fax: +39.040.938.0904. ORCID 0000-0002-7375-3666

*Livia E. Bove, present address E: liviaeleonora.bove@uniroma1.it ; T: +390649923477 ; Fax: +33.1.4427.3785. ORCID 0000-0003-1386-8207

ACKNOWLEDGMENT

We thank the *Agence Nationale de la Recherche* within the Blanc International programme PACS (reference ANR-13-IS04-0006-01) for financing this study and supported by the French state funds managed by ANR (project ANR-09-BLAN-0018-01). The inelastic neutron scattering experiments were performed at the IN1-LAGRANGE (Experiment 6-02-563; doi:10.5291/ILL-DATA.6-02-563), and the neutron diffraction experiments were performed at D4 (Experiment 6-07-10; doi: 10.5291/ILL-DATA.6-07-10), both in the Institut Laue-Langevin (ILL). The far- and mid-infrared spectroscopy experiments were performed at AILES beamline (Proposal Number: 2016566) in the Synchrotron SOLEIL. We acknowledge the synchrotron beam time allocated for this study by the Soleil scientific proposal committee in the framework of the CNRS RECIPROCS network (project 20160753), and Pierre Fertey for assistance during the measurements at the CRISTAL beamline. We thank Lise-Marie Chamoreau and Dominique Granier (*Réseau Rayons X et γ de l'Université de Montpellier*) for helping with single-crystal X-ray diffraction measurements at 100 and 135 K, respectively. Also, we thank Dr. Eleonora Stefanutti for the helpful discussion on the vibrational data.

References

(1) Gelb, L. D.; Gubbins, K. E.; Radhakrishnan, R.; Sliwinska-Bartkowiak, M. Phase separation in confined systems. *Rep. Prog. Phys.* **1999**, *62*, 1573.

(2) Klein, J.; Kumacheva, E., Confinement-induced phase transitions in simple liquids. *Science* **1995**, *269*, 816.

(3) Deville, S., Saiz, E., Nalla, R. K., Tomsia, A.P. Freezing as a Path to Build Complex Composites. *Science* **2006**, *311*, 515.

(4) Coussy, O. Mechanics and Physics of Porous Solids, Wiley, New York **2010**.

(5) Coasne, B.; Galarneau, A.; Pellenq, R.J.; Di Renzo, F. Adsorption, intrusion and freezing in porous silica: the view from the nanoscale. *Chem. Soc. Rev.* **2013,** 7;42(9), 4141-71.

(6) Giovambattista, N.; Rossky, P.J.; De Benedetti, P.G. Effect of Temperature on the Structure and Phase Behavior of Water Confined by Hydrophobic, Hydrophilic, and Heterogeneous Surfaces. *J. Phys. Chem.* **2009**, *113*, 13723.

(7) Zangi, R.; Mark, A.E., Electrofreezing of confined water. *J. Chem. Phys*. **2003**, *119*, 1694.

(8) Koga, K.; Zeng, X. C.; Tanaka, H. Freezing of Confined Water: A Bilayer Ice Phase in Hydrophobic Nanopores. *Phys. Rev. Lett.* **1997**, *79*, 5262.

(9) Koga, K.; Gao, G.T.; Tanaka, H.; Zeng, X.C. Formation of ordered ice nanotubes inside carbon nanotubes. *Nature* **2001**, *412*, 802.

(10) Stefanutti, E.; Bove, L.E.; Alabarse, F.G.; Lelong, G.; Bruni, F.; Ricci, M. A. Vibrational dynamics of confined supercooled water. *J. Chem. Phys.* **2019**, *150*, 224504.

(11) Bernardina, S.D.; Paineau, E.; Brubach, J.-B.; Judeinstein, P.; Rouzière, S.; Launois, P.; Roy, P. Water in Carbon Nanotubes: the Peculiar Hydrogen Bond Network Revealed by Infrared Spectroscopy *J. Am. Chem. Soc.* **2016**, *138*, 33, 10437–10443.

(12) Müller, A. and Henry, M. Nanocapsule water-based chemistry. *C. R. Chimie.* **2003**, *6*, 1201–1208.

(13) Monet, G.; Paineau, E.; Chai, Z.; Amara, M.S.; Orecchini, A.; Jimenez-Ruiz, M.; Ruiz-Caridad, A.; Fine, L.; Rouziere, S.; Liu, L.-M.; Teobaldi, G.; Rols, S.; Launois, P. Solid wetting-layers in inorganic nano-reactors: the water in imogolite nanotube case. *Nanoscale Adv.* **2020**, *2*, 1869-1877.

(14) Alabarse, F. G.; Haines, J.; Cambon, O.; Levelut, C.; Bourgogne, D.; Haidoux, A.; Granier, D.; Coasne, B. Freezing of water confined at the nanoscale. *Phys. Rev. Lett.* **2012**, *109*, 035701-5.

(15) Alabarse, F. G.; Silly, G.; Haidoux, A.; Levelut, C.; Bourgogne, D.; Flank, A.-M.; Lagarde, P.; Pereira, A. S.; Bantignies, J.-L.; Cambon, O., et al. Effect of H_2O on the pressure-induced amorphization of $AlPO_4$-54•xH_2O. *J. Phys. Chem. C* ***2014***, *118*, 3651-3663.

(16) Bordin, R.; Krott, L.; Barbosa, M. High pressure induced phase transition and superdiffusion in anomalous fluid confined in flexible nanopores. *J. Chem. Phys.* **2014**, *141*, 144502.

(17) Alabarse, F. G.; Rouquette, J.; Coasne, B.; Haidoux, A.; Paulmann, K.; Cambon, O.; Haines, J. Mechanism of H_2O insertion and chemical bond formation in $AlPO_4$-54•xH_2O at high pressure. *J. Am. Chem. Soc.* **2015**, *137*, 584-587.

(18) Gavazzoni, C.; Giovambattista, N.; Netz, P.A.; Barbosa, M.C. Structure and mobility of water confined in $AlPO_4$-54 nanotubes. *J. Chem. Phys.* **2017**, *146*, 234509.

(19) Fabbiani, M.; Polisi, M.; Fraisse, B.; Arletti, R.; Santoro, M.; Alabarse, F.; Haines, J. "An in-situ x-ray diffraction and infrared spectroscopic study of the dehydration of $AlPO_4$-54". *Solid State Sciences*. **2020,** *108***,** 106378.

(20) Onate Martinez, J. De. ; McCusker, L.B. ; Baerlocher, C. Micropor. Mesopor. Mat. **2000** *34*, 99–113.

(21) Alabarse, F. G.; Brubach, J.-B.; Roy, P.; Haidoux, A.; Levelut, C.; Bantignies, J.-L.; Cambon, O.; Haines, J. $AlPO_4$-54 – $AlPO_4$-8 structural phase transition and amorphization under high pressure. *J. Phys. Chem. C* ***2015***, *199*, 7771-7779.

(21) Clark, R. C.; Reid, *J. S. Acta Crystallogr. A* **1995**, *51*, 887 – 897.

(22) CrysAlis PRO, version 171.37.31; Agilent Technologies Ltd: Yarnton, England, **2014**.

(23) Dolomanov, O. V.; Bourhis, L. J.; Gildea, R. J.; Howard, J. A.; Puschmann, H., *J. Appl. Crystallogr.* **2009**, *42*, 339 – 341.

(24) Sheldrick, G. M., *Acta Crystallogr. A* **2008**, *64*, 112 – 122.

(25) Sheldrick, G.M., *Acta Cryst.* **2015**, *C71*, 3-8.

(26) Fisher, H.E.; Barnes, A.C.; Salmon, P.S. Neutron and x-ray diffraction studies of liquids and glasses. *Rep. Prog. Phys.* **2006**, *69*, 233–299.

(27) Keen, D.A. A comparison of various commonly used correlation functions for describing total scattering. *Journal of Applied Crystallography*. **2001**, *34*, 172-177.

(28) Fischer, H.E.; Cuello, G.J.; Palleau, P.; Feltin, D.; Barnes, A.C.; Badyal, Y.S.; Simonson, J.M. D4c: A very high precision diffractometer for disordered materials. *Appl. Phys. A* **2002**, *74***,** S160-S162.

(29) Ockwig N. W.; Cygan R. T.; Hartl M. A.; Daemen L. L.; Nenoff T. M. Incoherent Inelastic Neutron Scattering Studies of Nanoconfined Water in Clinoptilolite and Heulandite Zeolites. *J. Phys. Chem. C*, **2008**, *112*, 13629–13634.

(30) Ockwig N. W.; Greathouse J. A.; Durkin J. S.; Cygan R. T.; Daemen L. L.; Nenoff T. M. Nanoconfined Water in Magnesium-Rich 2:1 Phyllosilicates. *J. Am. Chem. Soc*. **2009**, *131*, 8155–8162.

(31) Jimenez-Ruiz, M.; Ferrage, E.; Blanchard, M.; Fernandez-Castanon, J.; Delville, A.; Johnson, M. R.; Michot, L. J. Combination of Inelastic Neutron Scattering Experiments and ab Initio Quantum Calculations for the Study of the Hydration Properties of Oriented Saponites. *J. Phys. Chem. C*, **2017**, *121*, 5029.

(32) Jimenez-Ruiz M.; Ivanov, A.; Fuard, S. LAGRANGE - the new neutron vibrational spectrometer at the ILL. *Journal of Physics: Conference Series* **2014**, *549*, 012004.

(33) Ivanov, A.; Jimnez-Ruiz, M.; Kulda, J. IN1-LAGRANGE - the new ILL instrument to explore vibration dynamics of complex materials. *Journal of Physics: Conference Series* **2014**, *554*, 012001.

(34) Roy, P.; Brubach, J.-B.; Calvani, P.; de Marzi, G.; Filabozzi, A.; Gerschel, A.; Giura, P.; Lupi, S.; Marcouillé, O.; Mermet, A., et al. Infrared synchrotron radiation: from the production to the spectroscopic and microscopic applications. *Nucl. Instr. & Meth. in Phys. Res. Sect. A* **2001**, *467*, 426-436.

(35) Bernardina, S. D.; Alabarse, F.; Kalinko, A.; Roy, P.; Vita, N.; Hienerwadel, R.; Berthomieu, C.; Judeinstein, P.; Zanotti, J.-M.; Bantignies, J.-L., et al. Experimental ensembles used to study the dynamics of water trapped in various media on the AILES beamline of SOLEIL synchrotron. *Vib. Spectrosc.* **2014**, *75*, 154-161.

(36) Poulet, G., Tuel, A., Sautet, P., A Combined Experimental and Theoretical Evaluation of the Structure of Hydrated Microporous Aluminophosphate AlPO4-18. *J. Phys. Chem. B*, **2005**, *109*, 22939.

(37) Perdew, J.P.; Burke, K.; Ernzerhof, M. Generalized Gradient Approximation Made Simple. *Phys. Rev. Lett.* **1996**, *77*, 3865-3868.

(38) Calandrini, V.; Pellegrini, E.; Calligari, P.; Hinsen, K.; Kneller, G.R. nMoldyn - Interfacing spectroscopic experiments, molecular dynamics simulations and models for time correlation functions. *JDN* **2011**, *12*, 201.

(39) Kuhs, W. F.; Lehman, M. S. *J. Phys. Chem.* **1983**, *87*, 4312.

(40) Garcia-Pérez, E.; Parra, J.B.; Ania, C.O.; García-Sánchez, A.; van Baten, J.M.; Krishna, R.; Dubbeldam, D.; Calero, S. A computational study of CO_2, N_2, and CH_4 adsorption in zeolites. *Adsorption* **2007**, *13*, 469–476.

(41) Fois, E. et al. *J. Phys. Chem. B* **2002**, *Vol. 106*, No. 18, 4806-4812.

(42) Kolesnikov, A.I.; Anovitz, L.M.; Mamontov, E.; Podlesnyak, A.; Ehlers, G. *J. Phys. Chem. B* **2014**, *118*, 47, 13414-13419.

(43) Saitta A. M.; and Datchi, F. Structure and phase diagram of high-density water: The role of interstitial molecules. *Phys. Rev. E* **2003**, 67, 020201(R).

(44) Rahman, A.; Stillinger, F.H. Molecular Dynamics Study of Liquid Water. *J. Chem. Phys.* **1971**, *55*, 3336.

(45) Catafesta, J.; Alabarse, F.; Levelut, C.; Isambert, A.; Hébert, P.; Kohara, S.; Maurin, D.; Bantignies, J.-L.; Cambon, O.; Creff, G., et al. Confined H_2O molecules as local probes of pressure-induced amorphisation in faujasite. *Phys. Chem. Chem. Phys.* **2014**, *16*, 12202-12208.

(46) Bove, L.E.; Klotz, S.; Strässle, Th.; Koza, M.; Teixeira, J.; Saitta, A.M. Translational and Rotational Diffusion in Water in the Gigapascal Range. *Phys. Rev. Lett.* **2013**, *111*, 18590.

(47) Parker, S. F.; Lennon, D.; Albers, P.W. Vibrational Spectroscopy with Neutrons: A Review of New Directions. *Applied Spectroscopy*, **2011**, *65(12)*, 1325 -1341.

(48) Li, J.C. Inelastic neutron scattering studies of hydrogen bonding in ices. *J. Chem. Phys.* **1996**, *105*, 6733-6755.

(49) Li, J. and Kolesnikov, A.I. Neutron spectroscopy investigation of dynamics of water ice. *J. Molec. Liq.* **2002**, *100/1*, 1-39.

(50) Crupi, V.; Majolino, D.; Migliardo, P.; Venuti, V. Neutron Scattering Study and Dynamic Properties of Hydrogen-Bonded Liquids in Mesoscopic Confinement. 1. The Water Case. *J. Phys. Chem. B* **2002**, *106*, 10884.

(51) Ramasay, J.D.F.; Lauter, H.J.; Tompkinson, Inelastic Neutron Scattering of Water and Ice in Porous Solids. *J. Journal de Physique Colloques.* **1984**, *45* (C7), C7-73-C7-79.

(52) Brubach, J.-B.; Mermet, A.; Filabozzi, A.; Gerschel, A.; Roy, P. Signatures of the hydrogen bonding in the infrared bands of water. *J. Chem. Phys.*, **2005**, *122, 184509*-7.

(53) Alabarse, F.; Silly, G.; Brubach, J.-B.; Roy, P.; Haidoux, A.; Levelut, C.; Bantignies, J.-L., Kohara, S.; Le Floch, S.; Cambon, O.; JHaines, J. Anomalous compressibility and amorphization in $AlPO_4$-17, the oxide with the highest negative thermal expansion. *J.Phys.Chem.C* **2017**, *121*, 6852−6863.

(54) Arakawa, M.; Kagi, H.; Fukazawa, H. Laboratory Measurements of Infrared Absorption Spectra of Hydrogen-Ordered Ice: A Step to the Exploration of Ice XI in Space, *ApJS*, **2009**, *184*, 361-365.

(55) Geiger, P.; Dellago, C.; Macher, M.; Franchini, C.; Kresse, G.; Bernard, J.; Stern J. N.; Loerting, T. Proton Ordering of Cubic Ice Ic: Spectroscopy and Computer Simulations. *J. Phys. Chem. C*, **2014**, *118*, 10989-10997.

(56) Zanotti, J.-M.; Judeinstein, P.; Dalla-Bernardina, S.; Creff, G.; Brubach, J.-B.; Roy, P.; Bonetti, M.; Ollivier, J.; Sakellariou, D.; Bellissent-Funel, M.-C. Competing coexisting phases in 2D water. *Sci. Rep*. **2016**, *6*, 25938.

(57) Chen, S.-H.; Liu, L.; Faraone, A. *Phys. Rev. Lett.* **2006**, *97*, 189803.

(58) Alcoutlabi, M.; McKenna, G. B. Effects of confinement on material behaviour at the nanometre size scale. *J. Phys.: Condens.* Matt. **2005**, *17*, R461–R524.

(59) Findenegg, G.H.; Jahnert, S.; Akcakayiran, D. Andreas Schreiber. Freezing and Melting of Water Confined in Silica Nanopores. *Chem Phys Chem* **2008**, *9*, 2651 – 2659.